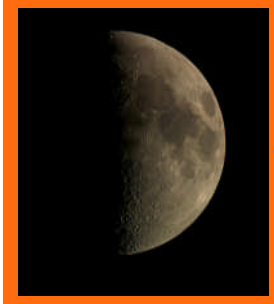

SELENOLOGY TODAY

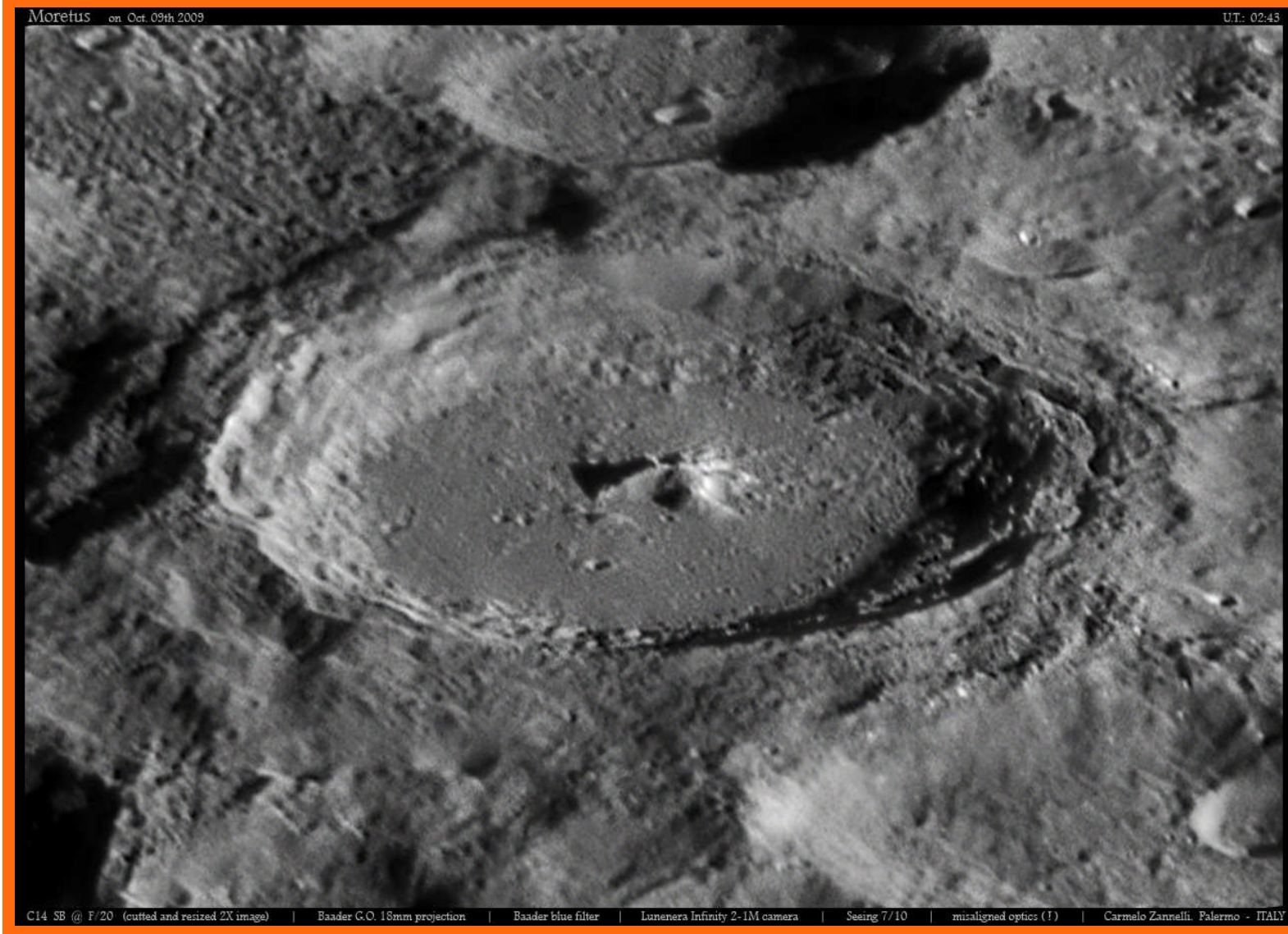

SELENOLOGY TODAY # 17

February 2010

http://www.glrgroup.eu/old/

Selenology Today is devoted to the publication of contributions in the field of lunar studies. Manuscripts reporting the results of new research concerning the astronomy, geology, physics, chemistry and other scientific aspects of Earth's Moon are welcome.

Selenology Today publishes papers devoted exclusively to the Moon.

The Selenology Today
Editorial Office
selenology_today@christian-woehler.de

Cover
Carmelo Zannelli

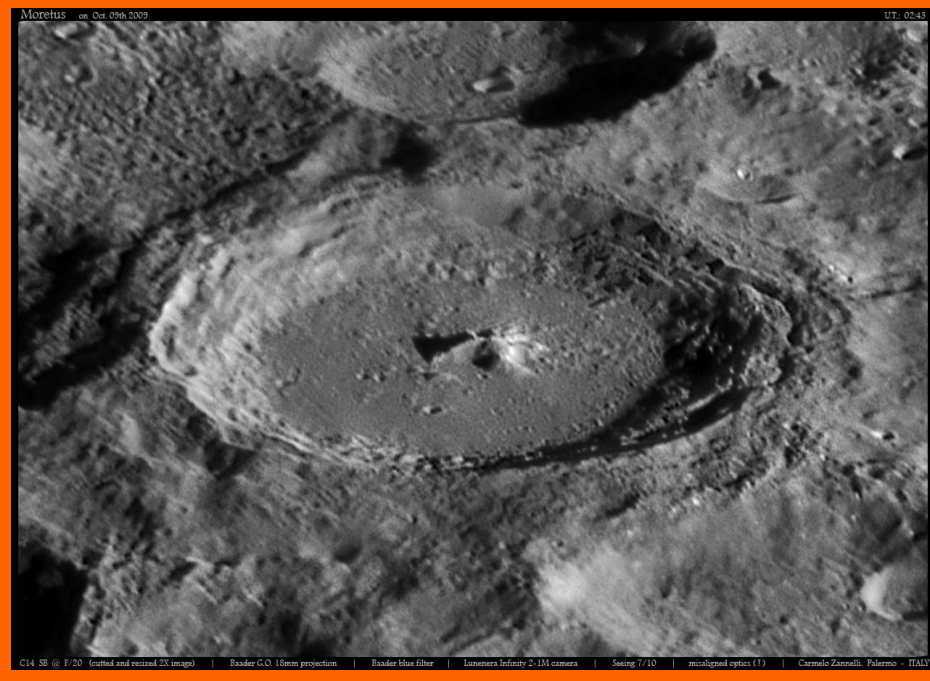

SELENOLOGY TODAY #17

February 2010

Selenology Today website

http://digilander.libero.it/glrgroup/

Application in lunar studies of simulations predicted from the Kaguya global DEM and LTVT software package.

By Raffaello Lena

Geological Lunar Research (GLR) Group

Abstract

The recent release of the Kaguya DEM, which is based on more than 6 million laser pings of the surface, provides a detailed enough map to use ray tracing to recreate any illumination. This paper includes simulations for Transient Lunar Phenomena (TLP) and digital lunar topography. Finally the article compares the accuracy and the convergence of the simulations predicted from the Kaguya global DEM obtained by the LTVT software package. Sometimes the detailed pattern of shadow spikes on the crater floor can be rather different than expected.

1.Introduction

Digital elevation maps (DEMs) are an important information source for many applications in planetary and lunar sciences, such as the description of local and regional topographic features, slopes and heights of lunar domes. For solving the DEM reconstruction problem by shape from shading (SFS) a variety of algorithms have been described in the literature. Information regarding the theory of the application of SFS can be found in Horn (1989) and Hapke (1993). Using a DEM we can estimate the surface slopes and hence can simulate the view seen from a given direction with lighting from some other specified direction.

The recent release of the Kaguya DEM, which is based on more than 6 million laser pings of the surface, provides a detailed enough map to use ray tracing to recreate any illumination:

https://www.soac.selene.isas.jaxa.jp/archive/

Mosher (2009) has updated the LTVT program so that it easily reads the DEM and rotates the virtual surface to exactly the lighting conditions at any instant. Mosher reports information about the kinds of simulations in

http://ltvt.wikispaces.com/Obtaining+Kaguya+DEM+data

These simulations will not look entirely realistic since they do not incorporate information on the way individual parts of the surface reflect light (the albedo and phase function) but, they will show which features will be in light and shadow. This paper includes several comparisons between real images and simulations predicted from the Kaguya global DEM obtained by the LTVT software package. Although the simulations are generally faithful, some discrepancies were found. Sometime the predicted shadows appear to be shorter or longer than the shadows actually observed, and the detailed pattern of shadow spikes on the crater floor can be rather different than expected.

2. Simulations about TLP reports

GLR group has previously observed a few historic TLP reports, finding that when the exact same illumination conditions (including librations) occur, that the TLP reappears. This proves that these particular TLPs are simply fleeting illuminations of a crater's floor that occur only with specific conditions. No levitating dust, gaseous discharges or other phenomena are required. The problem is that it may take an entire 18 year saros cycle for an exact repeat observation of any specific reported TLP, and there may be clouds on the night of interest. But now two advances in technology permit every entry in the TLP (Cameron, 1978) to be examined under conditions identical to each observation. Although the Cameron catalog include observational weights, recent publications about shadow effects (Lena and Cook, 2004; Lena et al., 2007) show how these can contribute to misinterpretation of TLPs, and imply that many of these rankings could be doubtful.

2.1 False TLP in Ptolemaeus entry #1380

I have used this capability to compare actual observations with a DEM-LTVT simulation for an event in Ptolemaeus (Lena and Cook, 2004). The NSSDC (National Space Science Data Center) catalog (Cameron, 1978) includes all reported phenomena regardless of the perceived weight of the observation. Entry #1380 describes an event recorded in Ptolemaeus by Bartlett on 3 November 1973 at 01:32 UT from Baltimore using a 10.8 cm reflector, x141 magnification.

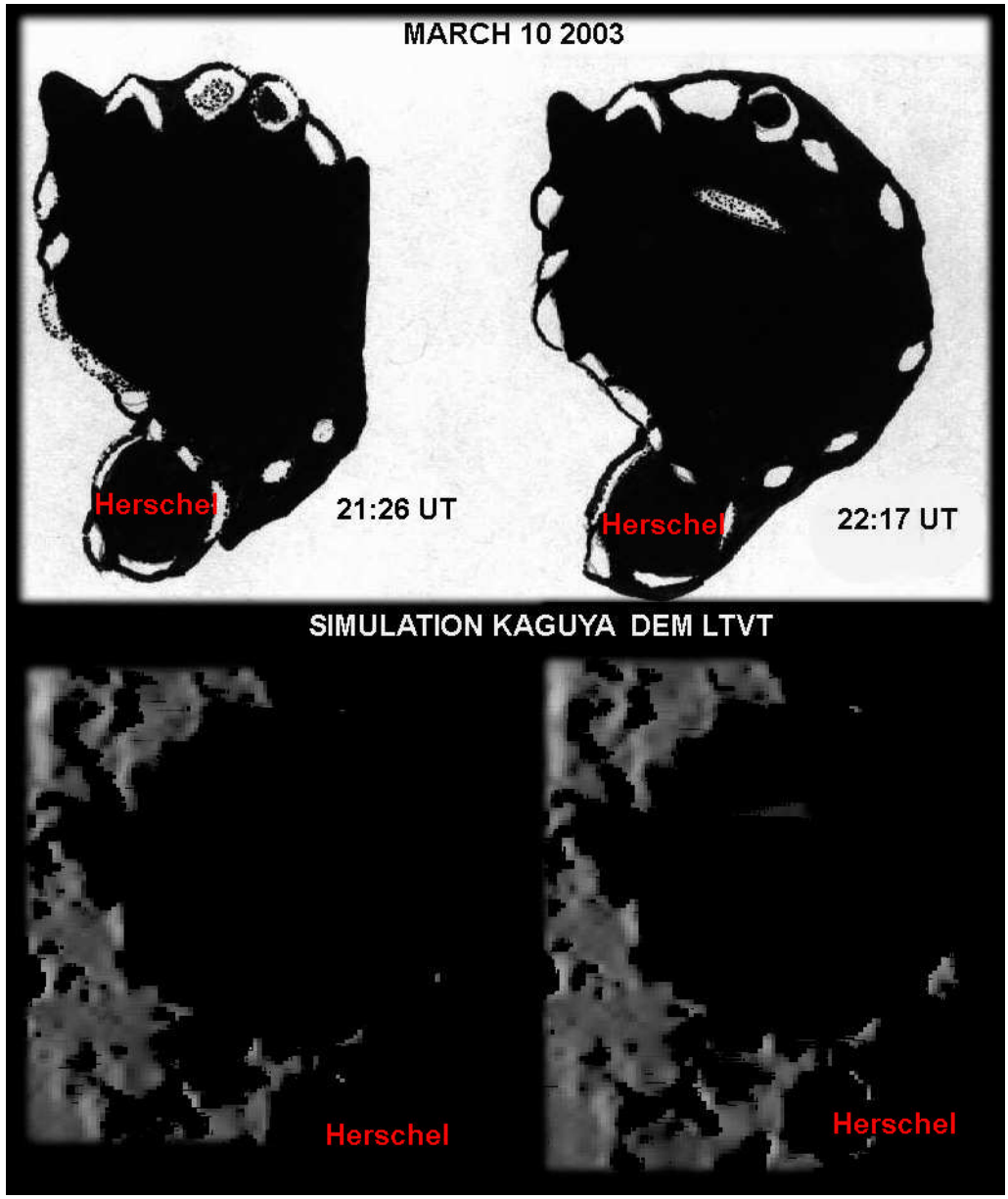

Figure 1. Observation carried out by Lena on March 10, 2003 at 21:26-22:17 UT. A 10 cm f/15 refractor was used. Below the simulation obtained with the Kaguya global DEM and LTVT software package.

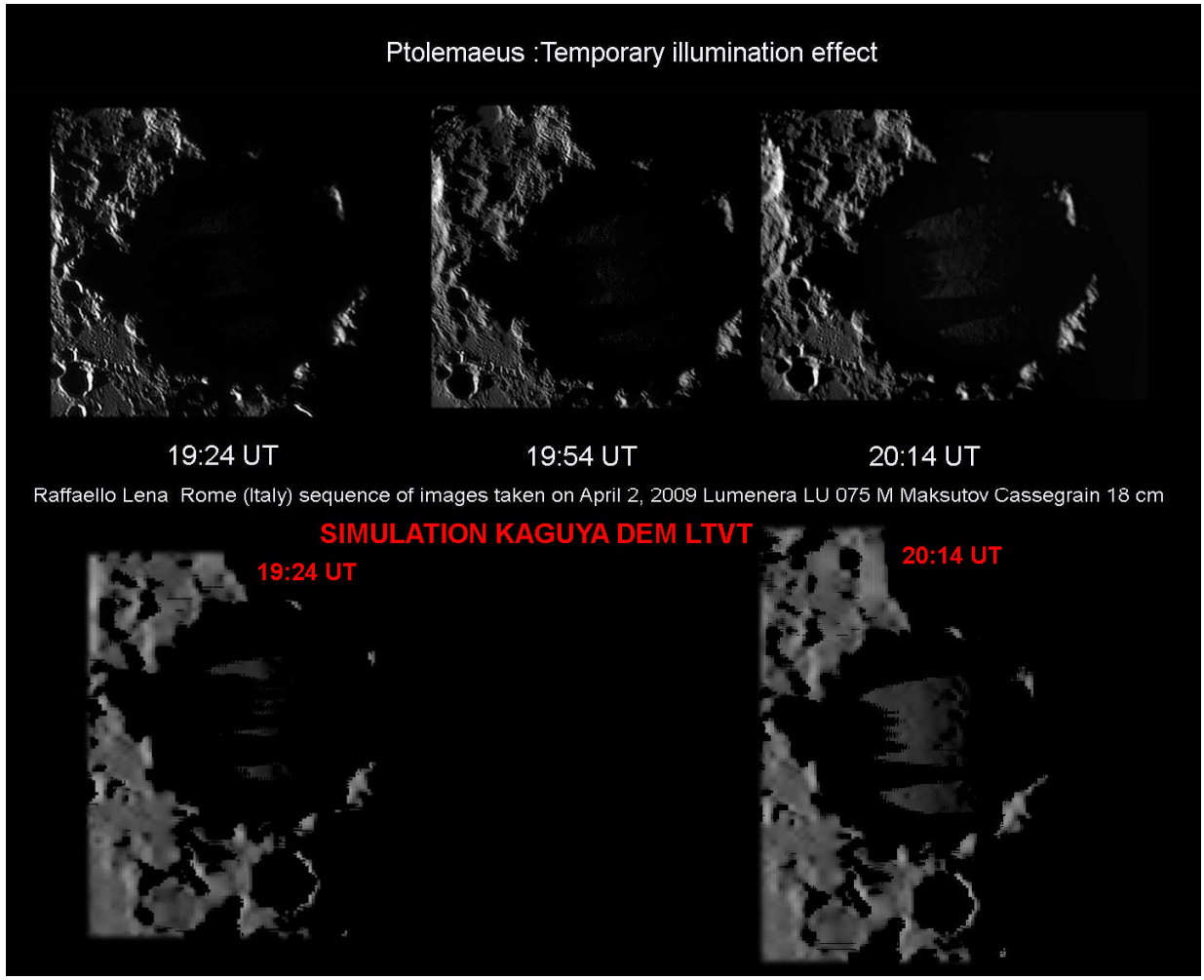

Figure 2. Images made by Lena on April 2 2009 at 19:24-20:14 UT (You may need to adjust your monitor to see the faint spots of the floor). Below the simulation obtained with the Kaguya global DEM and LTVT software package.

The event is quoted as a "Large oval bright area between center and S. wall though floor was in shadow. Looked like a feeble surface glow". Figure 1 shows a drawing of the author made in 2003 during an exact repeat of a classic Ptolemaeus haze report (cf. Lena and Cook, 2004). The simulation shows that the crater rim allows a swath of illumination to fall of the floor exactly as observed.

The image in Fig.2 displays that the temporary illumination of the floor can be shown by the simulation to be due to the geometry of rim and floor. This new capability can show which classic TLPs are repeatable, and which can not be explained that way.

2.2 False TLP in Alphonsus entry #705

Entry #705 in the catalog (Cameron, 1978) concerns an event recorded on Alphonsus by Poppendiek and Bond on 19 November 1958 at 04:00-04:30 UT from San Diego, using a 15 cm reflector, x370 magnification. The observers reported: "A diffuse cloud over central mountain, like a plume, very large compared with central peak".

Lena and Cook (2004) suggested strongly that small elevations seen under shallow illumination can appear as bright spots. This hypothesis is further supported by the recurrence of brightness as seen in observations made under the same specific lighting conditions. M. Cicognani took the image shown in Fig.3 on Aug 26, 2001 as part of the study closely mimics the 1958 report. Cicognani's image shows that the plume-like view reoccurs at exactly the same observing conditions, greatly reducing the possibility that the 1958 observation was a cloud. It actually was not a real Transient Lunar Phenomena but the transitory activity was of lighting that illuminates part of Alphonsus' central peak.

2.3 False TLP in Plato entry #1027

Lena et al. (2007) show that an observational Transient Lunar Phenomenon report concerning a Plato observation by Kelsey, on April 18 1967 (entry #1027 in the Cameron catalog), is not a TLP but the normal appearance of this crater. GLR group has studied Plato using observations made under illumination conditions that matched the event described by Kelsey illustrating the shape and the appearance of the observed streaks.

Figure 4a shows a drawing of the author made in 2003 during an exact repeat of a classic Plato streaks report (cf. Lena et al., 2007). The simulation (Fig. 4b) shows that the crater rim allows a swath of illumination to fall of the floor as observed.

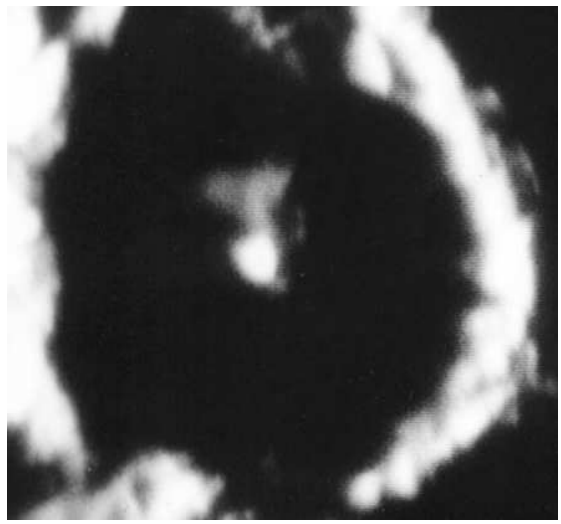

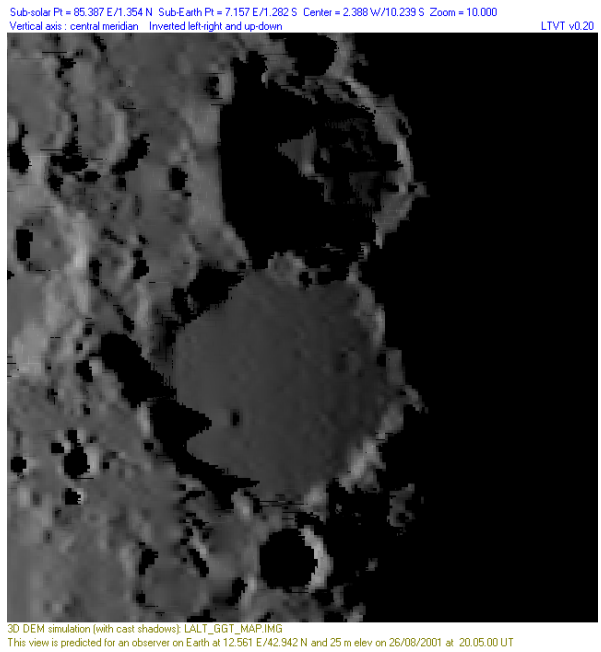

Figure 3. (Top) Image taken by Cicognani, August 26, 2001 at 20:05 UT using a 42 cm Cassegrain. (Bottom) The simulation obtained with the Kaguya global DEM and LTVT software package.

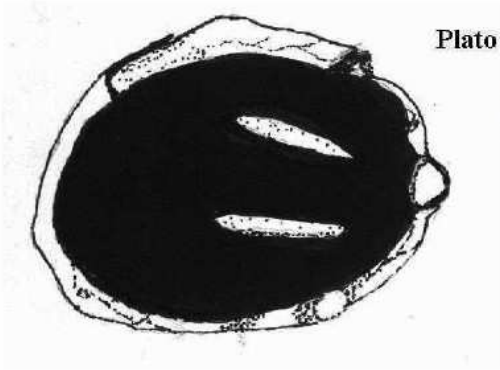

Fig. 4a: Drawing by Lena on May 9, 2003 at 18:25 UT

Figure 4a. Observation carried out by Lena on May 9, 2003 at 18:25 UT. A 10 cm f/15 refractor with a W 23 filter was used.

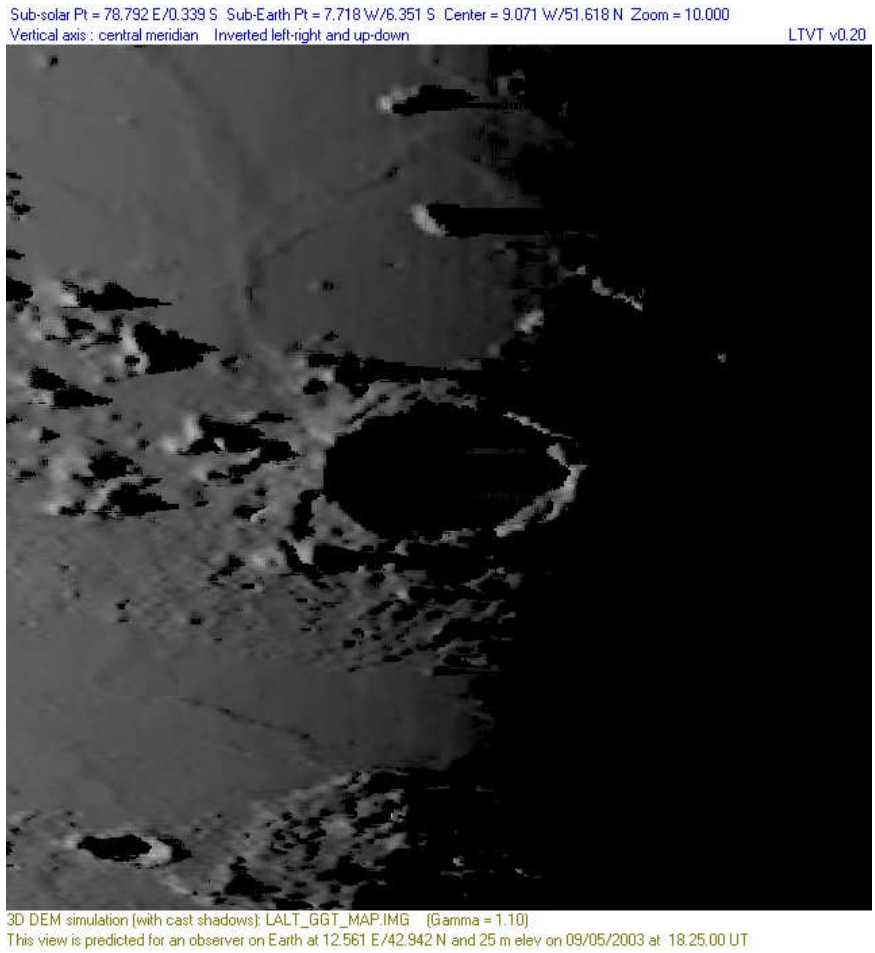

Figure 4b. The simulation obtained with the Kaguya global DEM and LTVsoftware package.

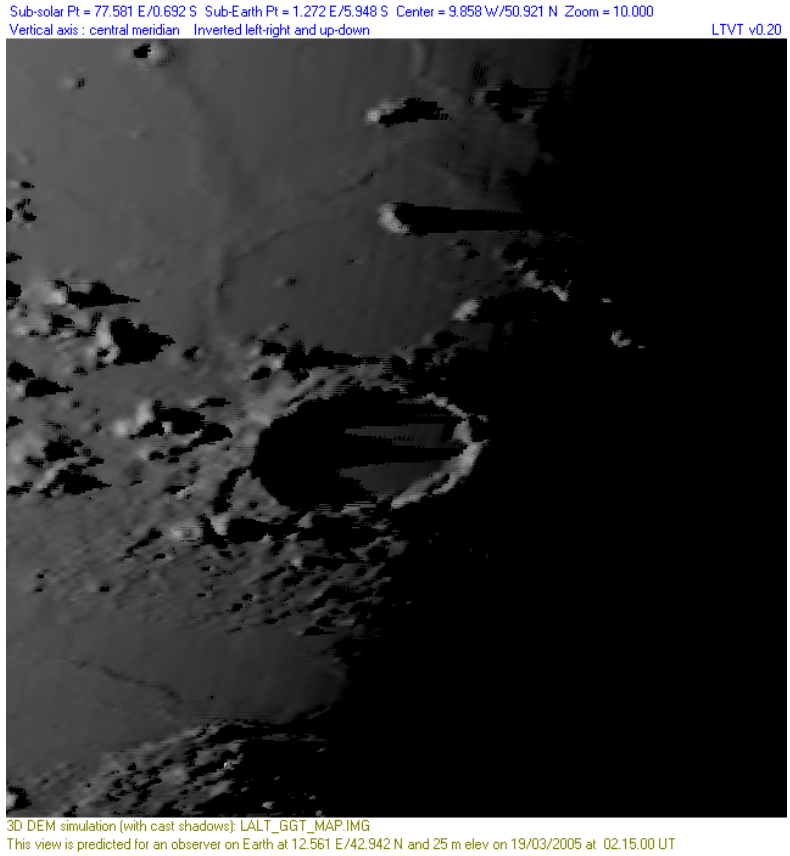

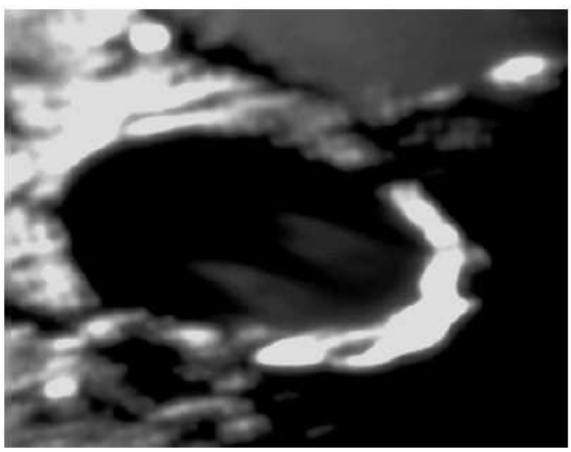

Fig. 5b: Plato streaks as imaged by Phillips on March 19, 2005 at 02:58 UT

Figures 5a and 5b. The false TLP reported by Kelsey on April 18, 1967 (entry #1027 in the Cameron catalog). To the top the simulation obtained with the Kaguya global DEM and LTVT software package.

Figures 5a and 5b show an image made by Phillips in 2005 during an exact repeat of a classic Plato streaks report (cf. Lena et al., 2007) and the simulation which displays that the temporary illumination of the floor can be shown by the simulation to be due to the geometry of rim.

Even with Plato the discrepancies in the shadow patterns suggest that some of the high and low points on the rim were missed. Presumably future missions, and possibly Kaguya's own stereo photos will fill in the gaps and make more accurate simulations possible. Despite its shortcomings, the Kaguya DEM seems to be capable of predicting the general characteristics of the lighting patterns seen on most crater floors with a good degree of accuracy.

3. Simulation about the Gamma peak's shadow in Plato

Observing Plato at the times when a curved appearance should have been detectable, GLR group was unable to demonstrate any curvature in the Gamma Peak's shadow. All our results (Lena et al., 2002) confirm that any curvature detectable in our images lasts only small intervals of time and is related to seeing-induced defocusing and deformations.

Figure 6a shows curvature in the shadow of the Gamma Peak. Figure 6b is one of several images taken by several other observers at the same time as Figure 6a but under better seeing conditions, and it shows no curvature. The shadow of the Gamma Peak can be seen to vary slightly in form from image to image related to seeing-induced defocusing and deformations. Because of these fluctuations, curvature in any of the images must be considered to be spurious. In particular, images with crisper detail show a straighter shadow (cf. Lena et al., 2002 and all images and references therein).

The shadow predicted from the Kaguya DEM (Fig.7) is similar to the straighter shadow of Fig. 6b.

4. Simulation about the O'Neill's Bridge and Yerkes

One of the better known lighting effects is the so-called O'Neill's Bridge, a classic "ray"-shaped fan of light that is seen as the Sun sets over the western shore of Mare Crisium. Discovered by John J. O'Neill, science editor of the New York Herald Tribune, July 29,1953, and studied by the selenographer H.P. Wilkins, it was originally thought to be an example of a natural bridge on the Moon. It can be best seen when the Moon is about

3 days past full. The “bridge” is now known, from Apollo-Lunar orbiter investigations, to be entirely illusory (cf. F. Graham, article reprinted in Selenology Today # 10, 2008).

Gus Johnson observed this area with a 3.2-inch Astrophysics f/11 refractor in 1987. We can see the shadow of what appears to be a bridge in his drawing: the fan of light seems to emerge from under a bridge in the constricted ridge area (see Fig. 8). A simulation of the region at a very low sun angle approximates the effect that originally gave rise to the name.

Figure 9 reports a dome (Yerkes 1) imaged under low solar altitude. This image was taken on October 31, 2004 at 11:15 UT by J. Phillips. The dome’s eastern flank does not show a black shadow but a dark grey shading (penumbra) of the dome’s flank, which represents grazing illumination by sunlight. On the whole the simulation seems accurate (Fig.10) but there are also some notable flaws in the Kaguya data and some predicted shadows are longer than really observed. Moreover, it does not contain the elevations necessary to produce the prominent observed shadow from Yerkes E, as visible comparing Figures 9 and 10. The discrepancies in the shadow patterns suggest that some of the high and low points in the Kaguya DEM were missed. Some shadows (marked in red arrow) appear too long; in a correct rendering part of the shadow would be blocked by the ridge.

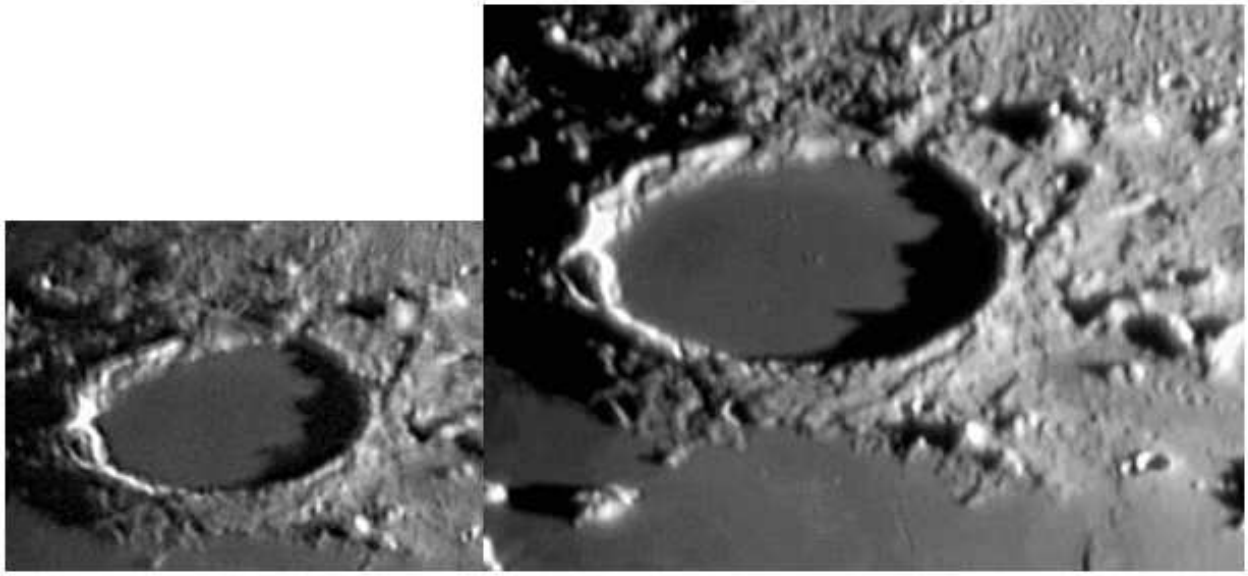

Figure 6a and 6b. The image on the left right corresponds to a lighting in which one of the spiky shadows cast by the east rim onto the floor has often been said to have a curved or "hooked" appearance but it was not confirmed by independent and contemporaneous image. On the left CCD image of Plato taken by A. Bares on 20 May 2002 at 20:11 UT UT with an HX516 camera fitted to a Mewlon Takahashi of diameter 250 mm at f/12. Seeing IV Antoniadi scale. On the right CCD image of Plato taken by C. Fattinnanzi on 20 May 2002 at 20:11 UT with a Vesta Pro webcam fitted to a Newton of diameter 200 mm at f/6. Seeing III Antoniadi scale. North to the top and West to the left.

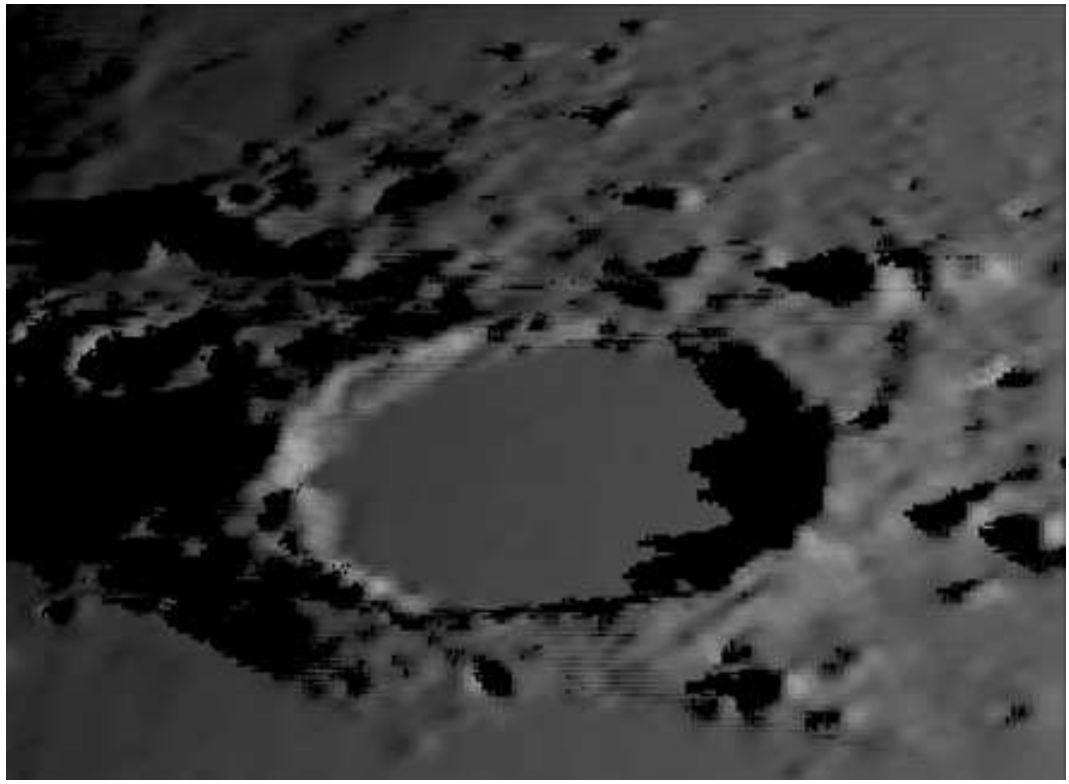

Figure 7. Simulation obtained with the Kaguya global DEM and LTVT software package for the date-time of figures 6a and 6b. North to the top and West to the left.

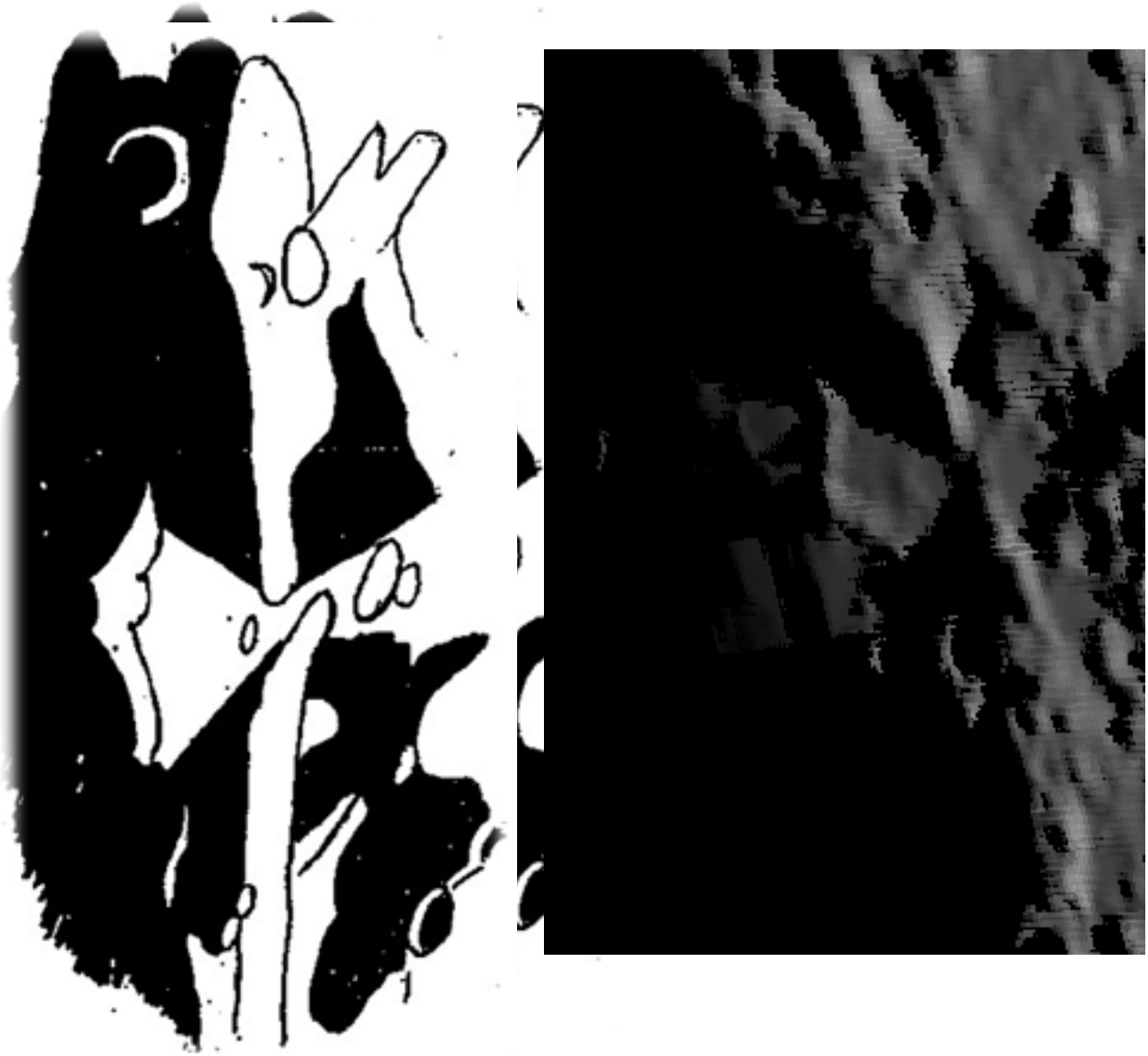

Figure 8. Gus Johnson observed this area on March 18, 1987 1:30-5.25UT. To the right the simulation obtained for the same date at 04:00 UT with the Kaguya global DEM and LTVT software package.

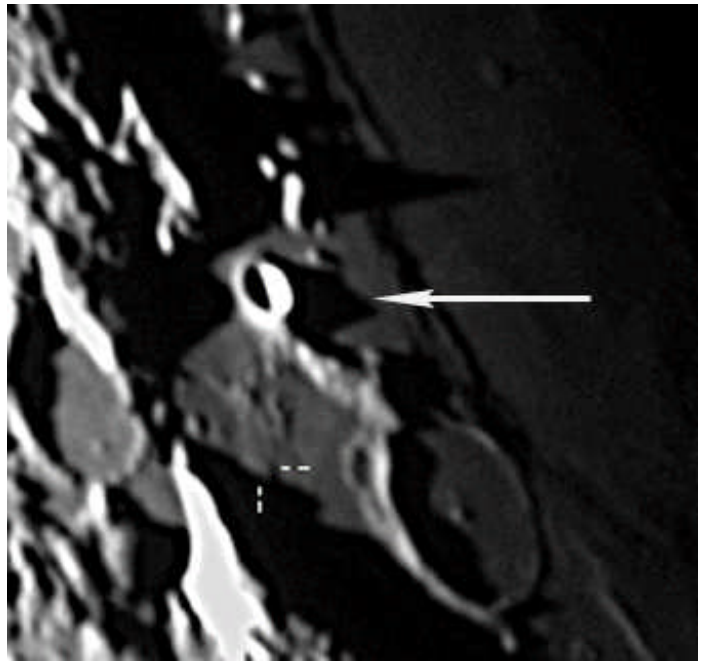

Figure 9. CCD image of Yerkes taken on October 31, 2004 at 11:15 UT by J. Phillips. White arrow shows the shadow from Yerkes E.

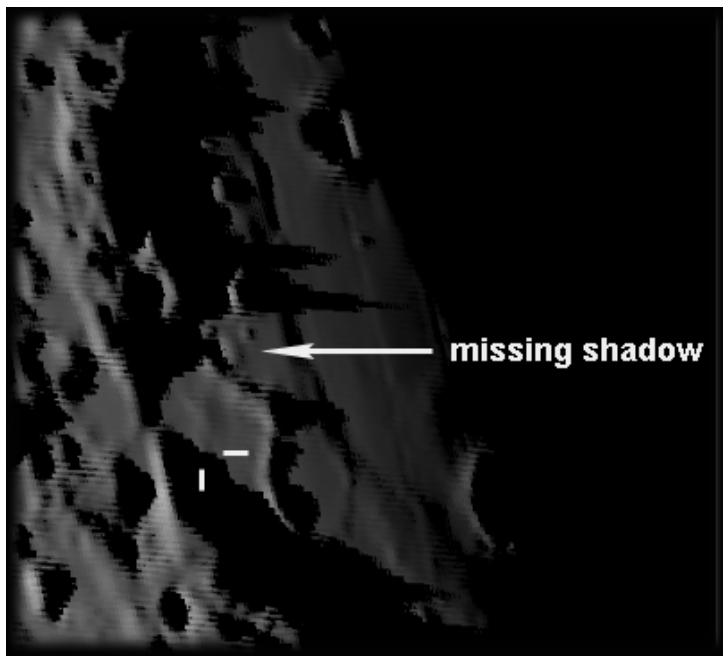

Figure 10. The simulation obtained with the Kaguya global DEM and LTVT software package, see text for detail. Some discrepancies in the shadow patterns suggest that some of the high and low points in the Kaguya DEM were missed.

5. Simulation about Mons Hansteen

Mons Hansteen is a well-known lunar red spot feature in the lunar highlands that has a distinctive arrowhead shape. The height of Mons Hansteen was computed using an image acquired under strongly oblique illumination (solar altitude of 2.1°) by K.C. Pau on December 9, 2008 at 13:20 UT (Fig. 11). The height amounts to 820 m and decreases towards the north and the south. The simulation obtained with the Kaguya global DEM and LTVT software package is shown in Fig. 12. The shadows predicted from the Kaguya DEM are similar to those observed.

6. Simulation about a dome near Aristillus

I have analyzed a dome, termed Aristillus 1 (Aris1), located near Aristillus, at longitude 5.67° E and latitude 33.28° N, with a diameter of about 43 km. The dome, of possible intrusive origin, is clearly apparent in the low-sun telescopic CCD image shown in Fig. 13. The simulation obtained with the Kaguya global DEM and LTVT software package is shown in Fig. 14.

In the corresponding simulation there are some notable flaws in the Kaguya data and some predicted shadows are shorter and of different shape than really observed. The discrepancies in the shadow patterns suggest that some of the high and low points in the Kaguya DEM were missed. Note the absence, in the DEM simulation, of the small crater Aristillus A. Effects such as that presumably arise because the raw laser height samples were likely too widely spaced to catch those features (Fig. 15).

Based on the telescopic CCD image shown in Fig. 13 it was obtained a DEM by applying the combined photoclinometry and shape from shading method. The resulting computation shows that the height of Aristillus 1 amounts to 85 m resulting in flank slope of 0.22°.

The computed height was compared to the height differences read from the Kaguya DEM at the same points. The resulting Kaguya height is lower yielding H=60 m.

7. Simulation about Archimedes

An image of Archimedes was taken by Lena on October 26, 2009 at 18:00 UT (Fig.16). The predicted shadows appear to be systematically shorter than the shadows actually observed, and the detailed pattern of shadow spikes on the crater floor is rather different than expected. Note the absence, in the DEM simulations, of some craters, Archimedes C and D (Fig.17). Effects such as that presumably arise because the raw laser height

samples were too widely spaced to catch those features. The Kaguya rim heights are systematically low and only vaguely correlated with the shadow spot measurements.

A difference of 600-900 m was computed comparing the computed height in the image shown in Fig. 16 and the height differences read from the Kaguya DEM at the same points (Fig. 17).

The lack of correlation may well arise from the interpolation of the original raw laser measurements at well defined, but irregularly spaced, points to the grid used for the global dataset. There might also have been some smoothing of the data which may have degraded the height of a relatively sharp feature like the crater rim.

Hence, the Kaguya central peaks heights are systematically low and not correlated with the shadow spot measurements (Fig. 20).

8. Simulation about Theophilus

Image of Theophilus was taken by Lena on December 29, 2007 at 03:30 UT (Fig.18). The predicted shadows cast from the central peaks appear to be shorter than the shadows actually observed (Fig. 19). The discrepancies in the shadow patterns of the central peaks suggest that some of the high points in the Kaguya DEM were missed. A difference of about 900-1000 m was estimated comparing the computed height of the central peaks in the image shown in Fig. 18 and the height differences read from the Kaguya DEM at the same points (Fig. 19).

The lack of correlation may well arise from the interpolation of the original raw laser measurements at well defined, but irregularly spaced, points to the grid used for the global dataset.

Figure 11. CCD image of Mons Hansteen taken by K.C. Pau on December 9, 2008 at 13:20 UT.

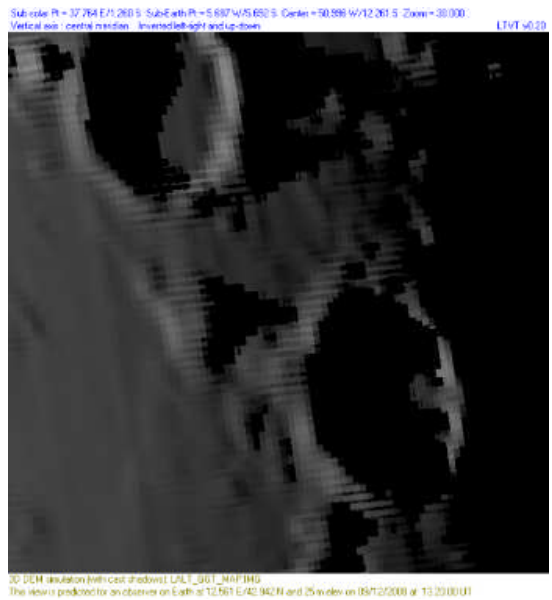

Figure 12. The simulation obtained with the Kaguya global DEM and LTVT software package, see text for detail.

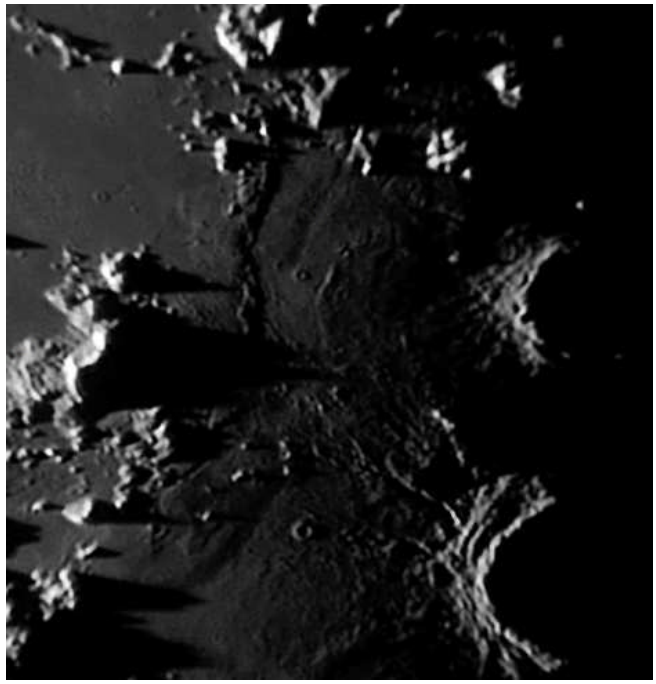

Figure 13. Image taken by Lena on May 1, 2009 at 19:30 UT.

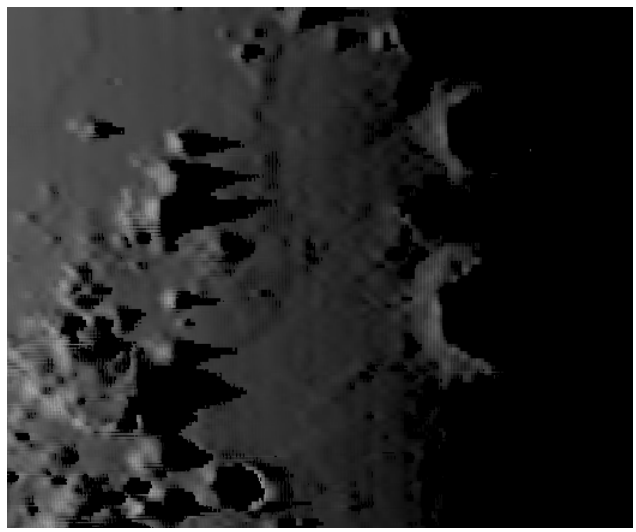

Figure 14. The simulation obtained with the Kaguya global DEM and LTVT software package.

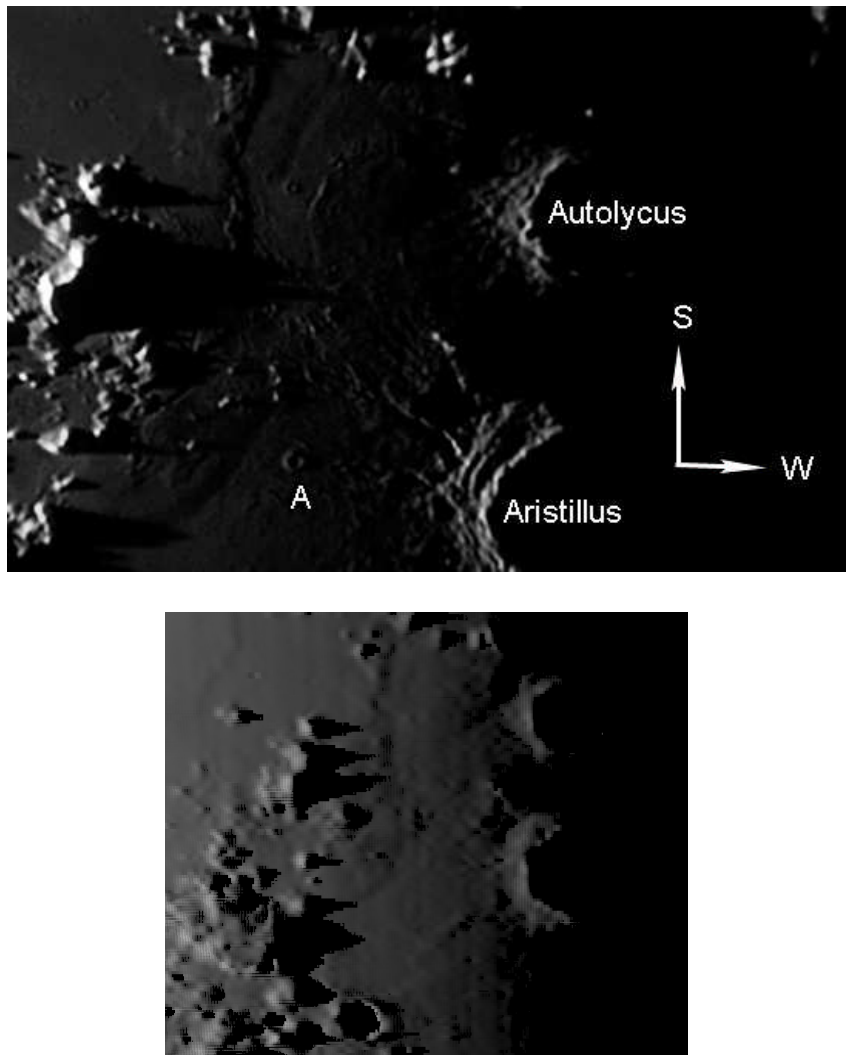

Figure 15. One way of testing the accuracy of the global DEM is compare the observed pattern of shadow and light with what is actually observed. In the case of the dome Aristillus 1 a divergence is present.

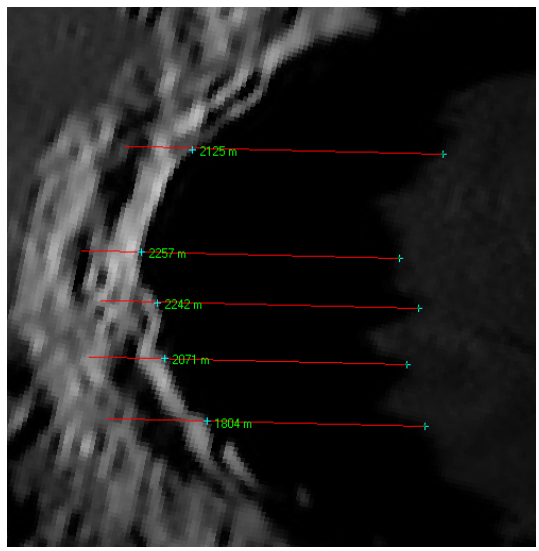

Figure 16. Image taken by Lena on October 26, 2009 at 18:00 UT and measurements.

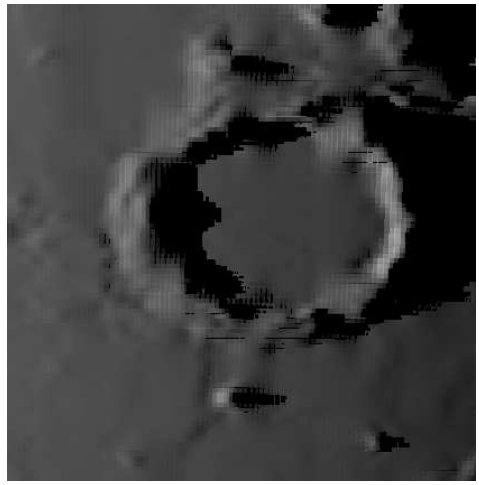

Figure 17. The simulation obtained with the Kaguya global DEM and LTVT software package. The predicted shadows appear to be systematically shorter than the shadows actually observed.

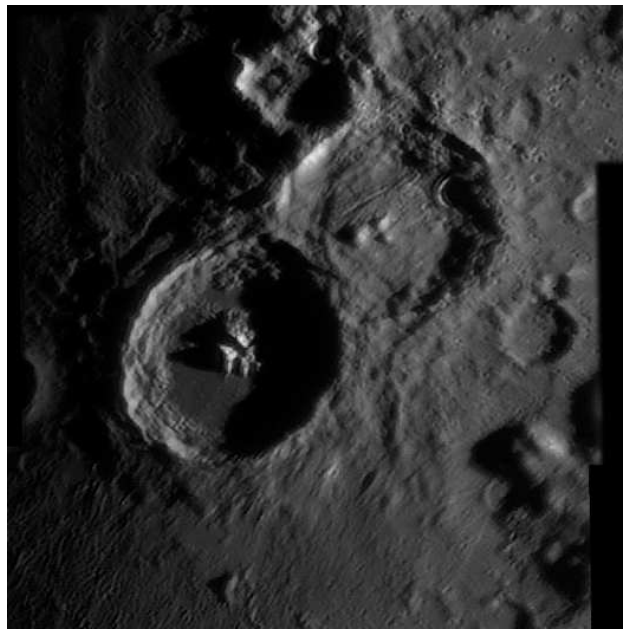

Figure 18. Image taken by Lena on December 29, 2007 at 03:30 UT

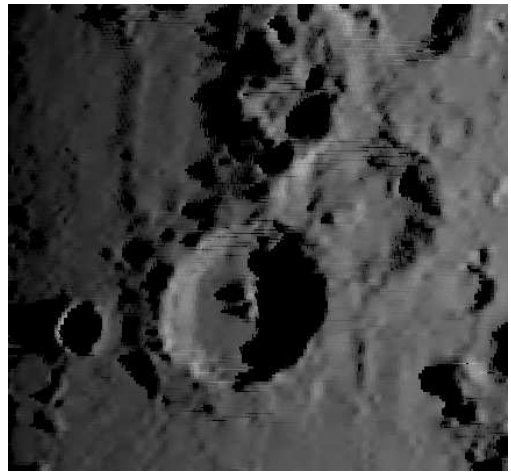

Figure 19. The simulation obtained with the Kaguya global DEM and LTVT software package.

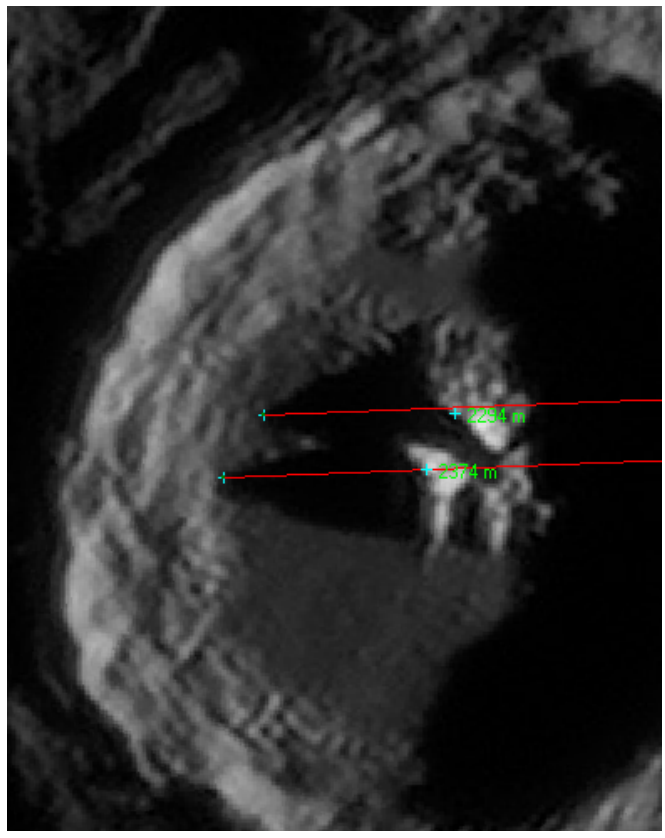

Figure 20. The heights of the central peaks computed from the image shown in Figure 18.

Acknowledgement: The author would like to thank Jim Phillips (GLR Group) for assistance and editing for improving the manuscript and C. Wood for his LPOD appeared on December 6, 2009.

References

[1] Cameron, W., Lunar Transient Phenomena Catalog, 1978, NSSDC, NASA-TM-79399, 109 pages.

[2] Graham, F., 2008. The O'neill Bridge:Discovery, Analysis and Subsequent Track in Literature to the Present (Reprinted). Selenology Today 10, pp. 34-40.

[3] Hapke, B., 1993. Theory of reflectance and emittance spectroscopy, Cambridge University Press, Cambridge, UK.

[4] Horn, B. K. P., 1989. Height and Gradient from Shading, MIT technical report, AI memo no. 1105A. http://people.csail.mit.edu/people/bkph/AIM/AIM-1105A-TEX.pdf

[5] Lena, R., Di Iorio, G., Bares, A., Fattinnanzi, C., Favero, G., 2002. Plato's Hook Part III: on the curvature of Gamma Peak's shadow on Plato's floor, The Strolling Astronomer, vol 44.4, pp. 37-43

[6] Lena, R., Cook, A., 2004. Emergence of low relief terrain from shadow: an explanation for some TLP. J. Brit. Ast. Assoc., 114, 136.

[7] Lena, R., Phillips, J., Bregante, M. T., Salimbeni, P.G., 2007. Local lunar sunrise in Plato-an explanation for some TLP Selenology Today, 8, pp. 30-53

[8] Mosher, J., 2009. LTVT http://ltvt.wikispaces.com/Obtaining+Kaguya+DEM+data

[9] Selene Data Archive, 2009 https://www.soac.selene.isas.jaxa.jp/archive/

Photometric observation of LCROSS Impact on the Moon

by Raffaello Lena, Jim Phillips and Ed Crandall

Geologic Lunar Research (GLR) group

Abstract

On October 9, 2009 at 11:39 19 UT the LCROSS vehicles impacted the Moon. Images taken by a wide variety of ground-based telescopes did not show a visible impact or the anticipated ejecta plume. LCROSS instruments captured all three phases of the Centaur impact: flash, ejecta plume, and crater. In this article we present the first data of our survey about photometric observations and some preliminary conclusions that can be drawn. The light curve is rather flat but shows, for both sequences analyzed, including Palomar images, a slight brightening just after the impact. A possible explanation is that the ejecta plume, originated by the LCROSS impact, produced only a slight brightening inside Cabeus, due to the topographical masking by lunar mountain M1.

1.Introduction

The impacts of meteorites or probes on the Moon give rise to a wealth of phenomena that can be detected. Both LCROSS vehicles successfully impacted the moon on schedule October 9th.

The primary goal of LCROSS was to measure the concentration of water ice (ice to dust ratio) in permanently shadowed lunar regolith. Setting constraints on water ice will set a fiducial for the LRO studies of hydrogen neutrons that are expected to have water ice as a source. Several important processes occur when a body strikes the lunar surface, including the initial impact, ejecta and plume dispersion, and the exposure of fresh subsurface

(cf. http://lcross.arc.nasa.gov/impact.htm). Initial video and images taken by a wide variety of space and ground-based telescopes

(http://www.universetoday.com/2009/10/09/moon-impact-data-and-images-from-lcross-first-glance/) did not show a visible impact or the anticipated ejecta plume.

Cabeus was chosen because it was inferred to contain a substantial amount of water ice. It was hoped by the LCROSS mission team that the impact would send an ejecta plume above the lunar surface, which could be observed from ground-based telescopes, but no plume was observed.

On the Lunar Reconnaissance Orbiter, which was observing the impact event from lunar orbit, the LAMP instrument (UV spectrometer) and the Diviner instrument (imaging radiometer) confirmed detection of (faint) ejecta plume in Cabeus. The nine LCROSS instruments captured all three phases of the Centaur impact: flash, ejecta plume, and crater. Thermal and mid infrared cameras showed the Centaur crater is about 28 m diameter. Ultraviolet and near infrared cameras and spectrometers detected a faint debris plume. The LRO Diviner thermal mapping instrument scanned the Centaur impact site about 2 hours before impact, 90 seconds after impact, and again about two hours after impact, clearly detected the impact site in all four thermal infrared channels.

Early results from the LCROSS instruments are summarized at

www.nasa.gov/mission_pages/LCROSS/main/LCROSS_impact.html and
www.nasa.gov/mission_pages/LCROSS/main/LCROSS_impact_images.html.

Images of the lunar crater Cabeus were taken on October 9, 2009 by the Palomar Observatory's 200-inch (5.1-meter) Hale Telescope and its adaptive optics system.

A time-lapse video of 12 minutes made with the Palomar telescope which can be carefully analyzed, was released to the public and displays the region of interest, centred on Cabeus

(http://www.astro.caltech.edu/palomar/lcross.html).

These high resolution images made with the Palomar telescope were extracted, analyzed and compared with the data acquired during our GLR survey.

In order to trace the light curve of the crater for any detection of brightness, the method of relative photometry has been used. Thus, if an intensity spike is detected simultaneously in three telescopes, at the same lunar coordinates, the increase of brightness could be considered a possible sign of the event. In this article we present the first data of this survey and some preliminary conclusions that can be drawn from the collected data.

2.Observations and data reductions

We will focus on the two instruments that were used during the survey.

The first one was a Refractor 110 mm f/6.5 APO telescope used with a 3X Barlow lens and a filter IR blocking. The AVI was taken with a Toucam CCD camera (Ed Crandall) from Lewisville (North Carolina, USA). The second telescope was a Refractor APO TEC 200mm f/8 telescope used at f/40 with an Orange (W#12) filter. The AVI was taken with a high-sensitivity Skynyx monochrome CCD camera with a frame rate of 32 frames per second (Jim Phillips) from Isle of Palms (South Carolina, USA). The telescopes were synchronized for timing using the countdown counter for the impact as released on October 8 2009 by NASA-LCROSS team. The AVIs were recorded some minutes before of the impact time which occurred on October, 9, 2009 at 11:39 19 UT. The single unprocessed raw frames were extracted from the AVI records and analyzed (the range of interval was comprised from 10 seconds before the impact to 40 seconds after the impact). Every sequence of images has been centred and measured with Astroart software package.

Simultaneously, the video images from the Palomar record released to the public were extracted and saved as BMP format. Unprocessed digital images, in RGB format, were analyzed by enclosing the three control zones (C1, C2, C3), the Cabeus region and the Sky by rectangular box and measuring the histogram average for the interior of the box (cf. Fig. 1).

The box was chosen no close to M1 ridgeline. In fact in all videos was seen “pixel bouncing” off the M1 ridgeline, both before, at and after the impact event. These effecrs were discounted as atmospheric turbulence seeing smears of photons emanating from the M1 ridgeline. It was calculated the ratio between the medium ADU (Analog to Digital Unites) value of the area inside Cabeus, in the region where the impact was predicted, with the medium ADU values of three control zones. The control zones are selected near Cabeus: all measured values were subtracted with the average value of the Sky. In this way it is possible to show eventual variations of Cabeus brightness, regarding the surrounding regions, eliminating the interferences due to changes of atmospheric transparency. The choice of three distinguished zones allows to control the small errors from zones of various sensibility of CCD sensor or deriving to mediate not on the same pixel.

Every point is the average of three points, everyone relative to a control zone. The error bar on every point is 5% of the value (Fig. 4).

Some images taken from Isle of Palms and Lewisville (USA) during our survey are shown in Fig. 2 and 3, respectively.

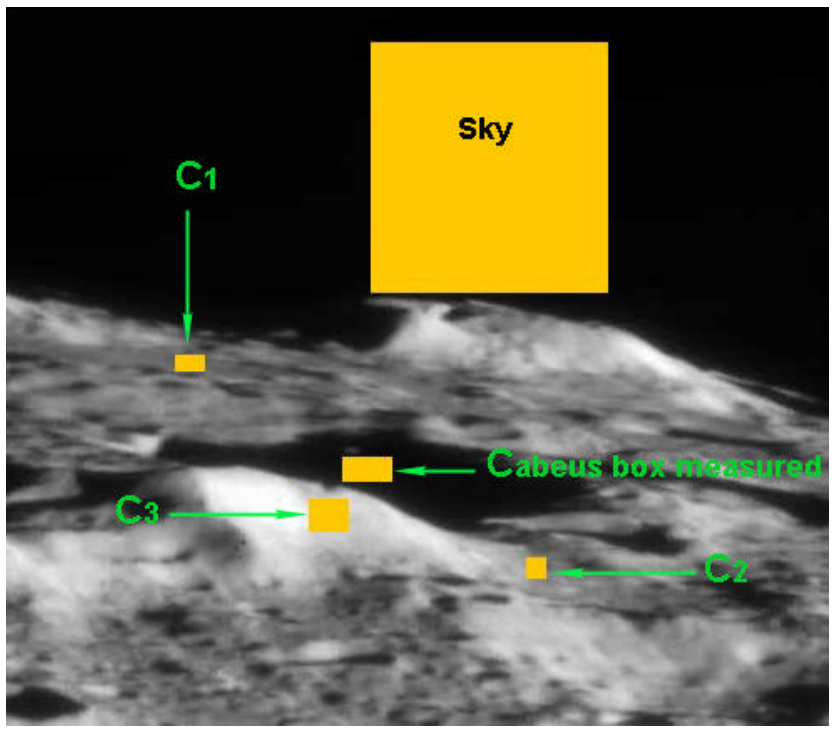

Fig.1. Region of Cabeus at the impact time (11:39 19 UT October 9, 2009). Unprocessed frame extracted by the record made with the Palomar telescope (courtesy of Palomar team). In the image are shown the three zones of comparison (C1-C3) used for relative photometry. The lunar mountain M1 is marked.

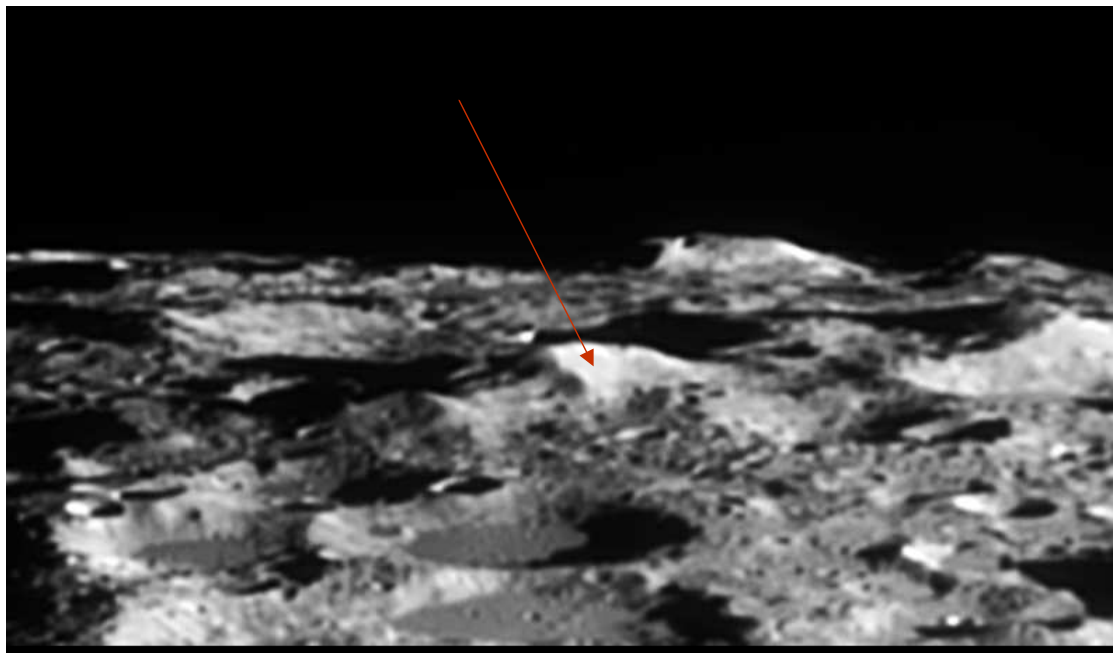

Fig.2. Region of Cabeus at the impact time (11:39 19 UT October 9, 2009). This image as unprocessed frame was used for relative photometry. The frame, here processed with Registax 5, was taken with an APO TEC 200mm f/8 telescope and a Skynyx monochrome CCD camera (Jim Phillips, Isle of Palms). The three zones of comparison were identified and measured as described in the text. The lunar mountain M1 is marked with a red arrow.

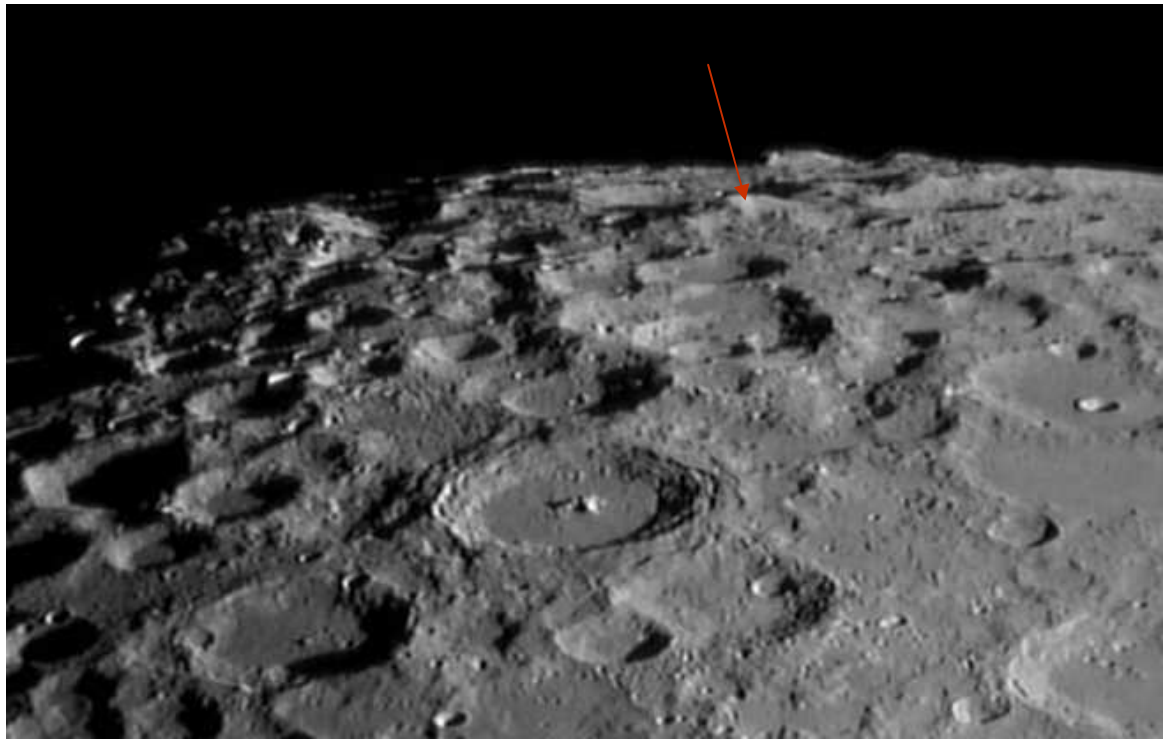

Fig.3. Region of Cabeus at the impact time. This image as unprocessed frame was used for relative photometry. The frame, here processed with Registax 5, was taken with an Refractor 110 mm f/6.5 APO telescope used with a 3X Barlow lens and a filter IR blocking. The AVI was taken with a Toucam CCD camera (Ed Crandall, Lewisville North Carolina, USA). The three zones of comparison were identified and measured as described in the text. The lunar mountain M1 is marked with a red arrow.

3.Measurements

The images reported in Fig.2 and 3 are processed images generated by stacking several hundreds of video frames using Registax software package.

For the photometric measurements unprocessed frames were selected from each video clip and converted into an 8 RGB BMP format. Several frames were extracted at specific times, as follows:

5 seconds and 1 second before impact, at Impact Time (11:31 19s UT October 9, 2009), and 5-10-20-30-40 seconds post impact. Frames degraded by seeing were excluded because of the impossibility to take measurements. Cabeus was identified on each selected frame and a histogram greyscale value average with standard deviation was obtained for the boxed area corresponding to the region of the impact. The process was then repeated for the corresponding three control zones (C1, C2, C3). An initial relative

photometric plot of the ratio value versus the time was made using Microsoft Excel software. The light curve is reported in Fig.4. The relative shadow intensity is brighter in our images than in the Palomar images, because there is light scattered into the shadow inside the telescope due to the lower resolution.

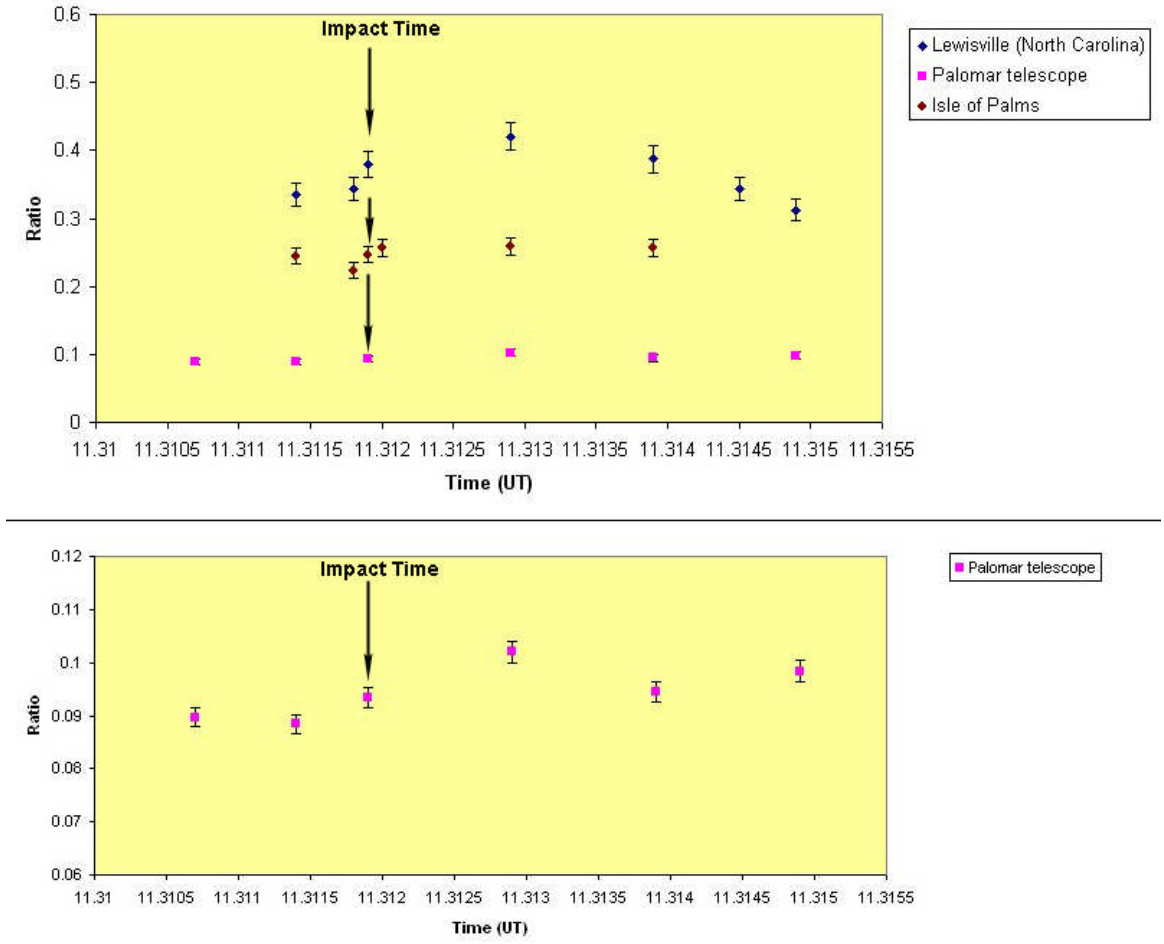

Figure 4. Light curve obtained with relative intensity versus time. Every point is the average of three measures. The error bar is 5%. Below the scaled curve on the y axis for Palomar images.

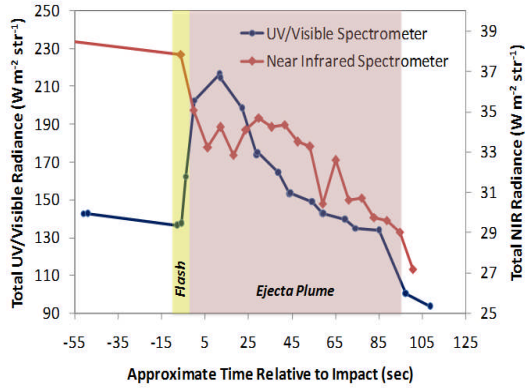

Figure 5. The total integrated radiance (integrated across all wavelengths measured by each spectrometer) as a function of time relative to the approximate impact time and its variation (LCROSS team).

4.Results and discussion

4.1 LCROSS analysis

LCROSS analysis showed a thermal image of a warm impact crater about 18-20m in diameter

(http://www.nasa.gov/mission_pages/LCROSS/main/LCROSS_impact_images.html).

The Ultraviolet (UV)/Visible and Near Infrared down-looking spectrometers monitored the flash of the impact, the ejecta plume and the reflectance off the floor of Cabeus. Fig. 6 (released by LCROSS team) shows the total integrated radiance (integrated across all wavelengths measured by each spectrometer) as a function of time relative to the approximate impact time and its variation.

4.2 Photometric observations

The light curve reported in Fig.4 is rather flat and there was no evidence of a visible flash or ejecta plume. Both sequences show a slight brightening just after the impact, occurring approximately at the same time (see Fig.4, and the scaled curve on the y axis, which emphasize the slight increase of the relative intensity, for Palomar images). These results can be interpreted as being somewhat ambiguous.

However, a minor increase of brightness, detectable 10 seconds post impact, cannot be excluded as not real and could possibly be the result of a faint ejecta. A slight increase of the relative intensity was also measured 1 second post impact time in our photometric measures using the frames taken from Isle of Palms. The results show that the ejecta produced by the impact was really very faint and the slight intensity increase is not a certain detection.

A possible explanation of our data is that the ejecta plume, originated by the LCROSS impact (Fig 5) produced only a slight brightening inside Cabeus (Fig.4) due to the topographical masking by lunar mountain M1.

In this scenario the predicted sunlight-topography model was not correct and the curtain never reached the sunlight. The plume was blocked from Earth view because the first ejecta to reach sunlight is hidden by the flank of M1.

Imbrium Ejecta Flow Pattern

by Stefan Lammel

Geologic Lunar Research (GLR) group

Introduction

The ejecta flows discussed here are broadly in an area known as the Haemus Mountains to the south of the Imbrium Basin.

The Imbrium event occurred about 3.8 billion years ago, excavating a depression 1160 km in diameter and blanketing much of the lunar surface with debris ejected by the impact. The basin was subsequently flooded by lava flows to form the relatively smooth surface known as Mare Imbrium. The Apennine Mountains form the south-eastern rim of the basin, the bulk of this mountain chain consists of giant blocks of lunar crust that were lifted and tilted outward by the impact and then covered by an unknown thickness of debris ejected from the basin (cf. Schultz, 2001; Wood, 2009). The more hummocky deposits were probably formed by the base surge, a turbulent cloud of fluidized debris that moved outward along the surface from the point of impact. The hummocks resemble huge dunes, their dimensions indicate a velocity of flow in excess of 100 km/hr and a maximum thickness of the deposits of several kilometres (Masursky et al., 1978). Further information about the origin of Imbrium basin are given in The-Moon Wiki (http://the-moon.wikispaces.com/Mare+Imbrium).

The Haemus Mountains

The Haemus Mountains (Fig. 2) bound the south-western edge of Mare Serenitatis and form part of the rim of the Serenitatis basin, they have a strongly lineated pattern which is radial to the Imbrium basin. Carr (1966) described the mountains as composed mostly of ejecta from the Imbrium basin. The lineation may be due to shattering of the lunar crust by the Imbrium impact event, depositional fluting of the ejecta, gouges made by impacting debris from the Imbrium basin, or a combination of the three.

Observing Session

It was about half an hour after dawn and I was reluctantly about to pack up, the seeing was still good but I had just used up all the available disk space on my laptop (my external disk had failed a few days earlier). I decided to take one last look at the part of the terminator that I had so far ignored and as I did so this scene came into view and I knew I had to capture it whatever it took. It was a great moment, as I scanned northwards the lighting over the Haemus Mountains was so dramatic.

Just above where I had started that morning and there it was, the Hadley

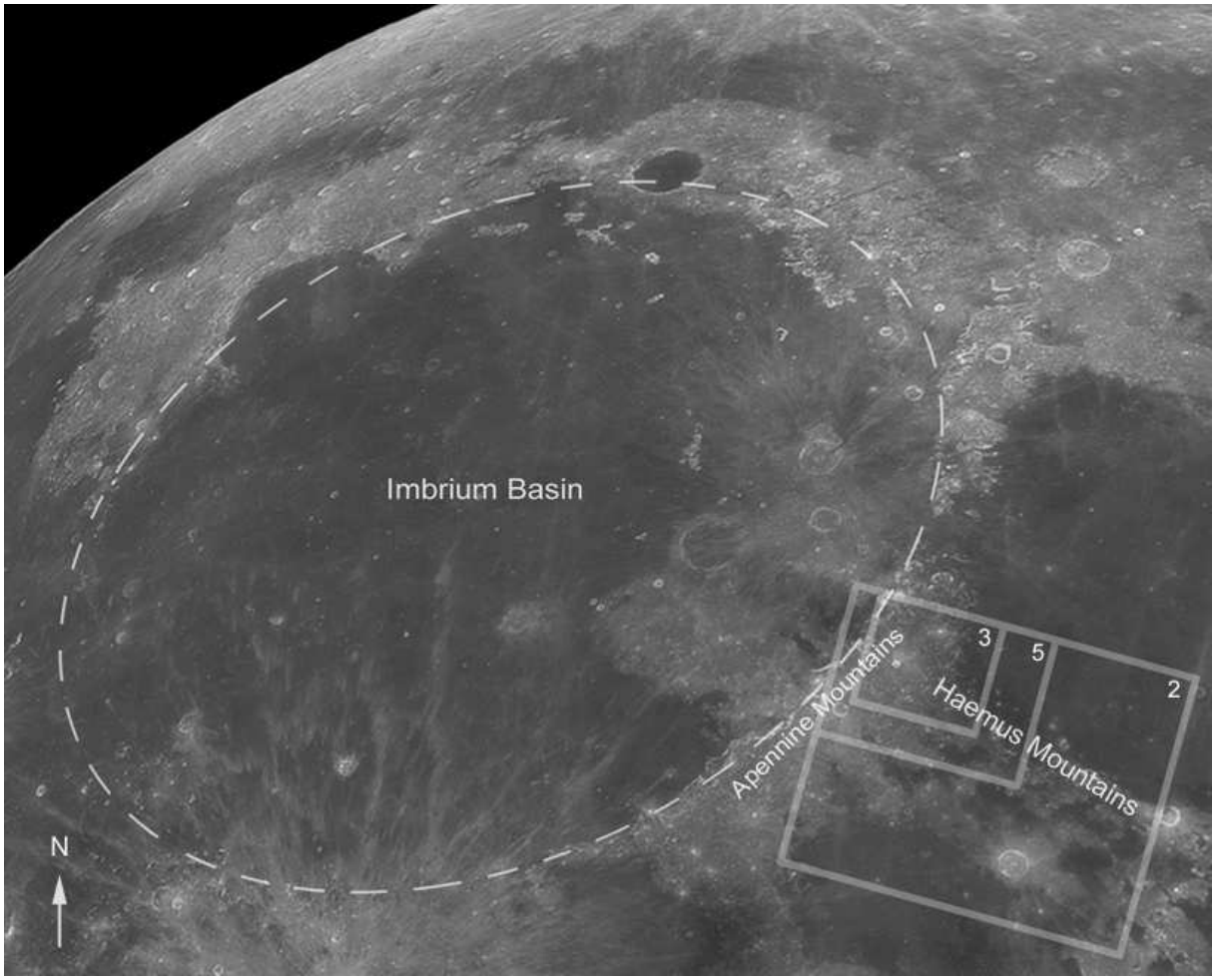

Figure 1. The Imbrium Basin. The numbered rectangles show the location of the figures below.

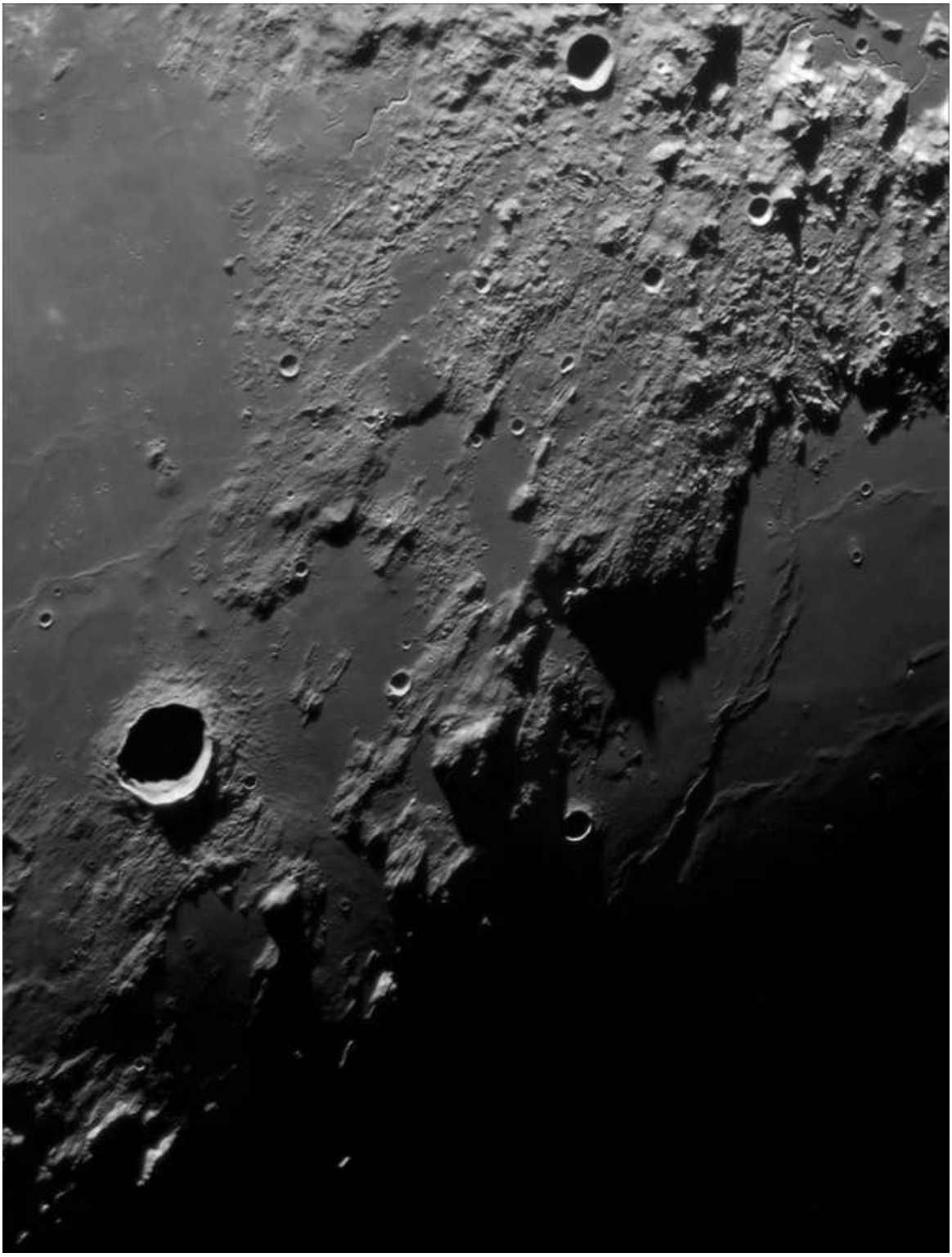

Figure 2. The Haemus Mountains (shown west up, as are all subsequent images).

Rille perfectly placed in the top left corner and the mountain peaks catching the evening sun in a diagonal to the bottom right. But there was no disk space left on the laptop so I had a problem, what to do? Well fortunately I was able to record just enough frames to a memory card which I quickly removed from a digital camera, there's a first time for everything! The lighting was new to me for this area which always adds interest and, as it has turned out, despite the daylight recording and high gain the resulting image was certainly worthwhile.

Image details

Scope: 10in f 4.8 Newtonian

Camera: Lumenera Infinity 2-1M, Televue Powermate 5x, Astronomik green filter

Processing: Avistack, Registax5, Photoshop Elements 5, Focus Magic

Discussion

A Possible Ejecta Flow Pattern?

I don't know if this has been discussed before but I see a pattern in the flow of ejecta from the Imbrium impact beyond the Apennines (Fig. 3). It was great to see this splurge of debris, I'm not sure I had fully recognized this one overlapping the more obvious one below it before, it looks so fresh as if it's been captured mid flow. Could this be a recognized type of flow pattern with these separate flow fingers splaying out from the main thrust, perhaps seen in avalanches or mud or rock slides on Earth? What would cause a flow to splay out like this? Is it related to flow dynamics or perhaps it is more likely that some extraneous event has influenced the flow? Perhaps a secondary impact landed on the flow as it advanced, but the fingers further back would not fit with that. So alternatively, perhaps it is possible that a stream of debris (similar to that which created the Copernicus secondary crater chains for example) landing on top would do it, perhaps even helping to explain the deep crevice along the centre of the flow and the slightly S curved shape. It has to be admitted however, that such a coincidence of timing and alignment might well seem unlikely. The flow fingers that appear to emanate from the crevice further back are less clearly defined and therefore more speculative than those at the front of the flow. Looking at Lunar Orbiter images of the area (Fig. 4) perhaps it's not too surprising that there is not much to see of this pattern, due to the higher angle of illumination the fingers at the front of the flow are barely detectable. Similarly the Clementine colour ratio view of the area (Fig. 4) does not give much away about this possible formation either. Lower angle lighting is more helpful in interpreting the terrain and with such lighting it can be seen that the flow appears more rubbly than its

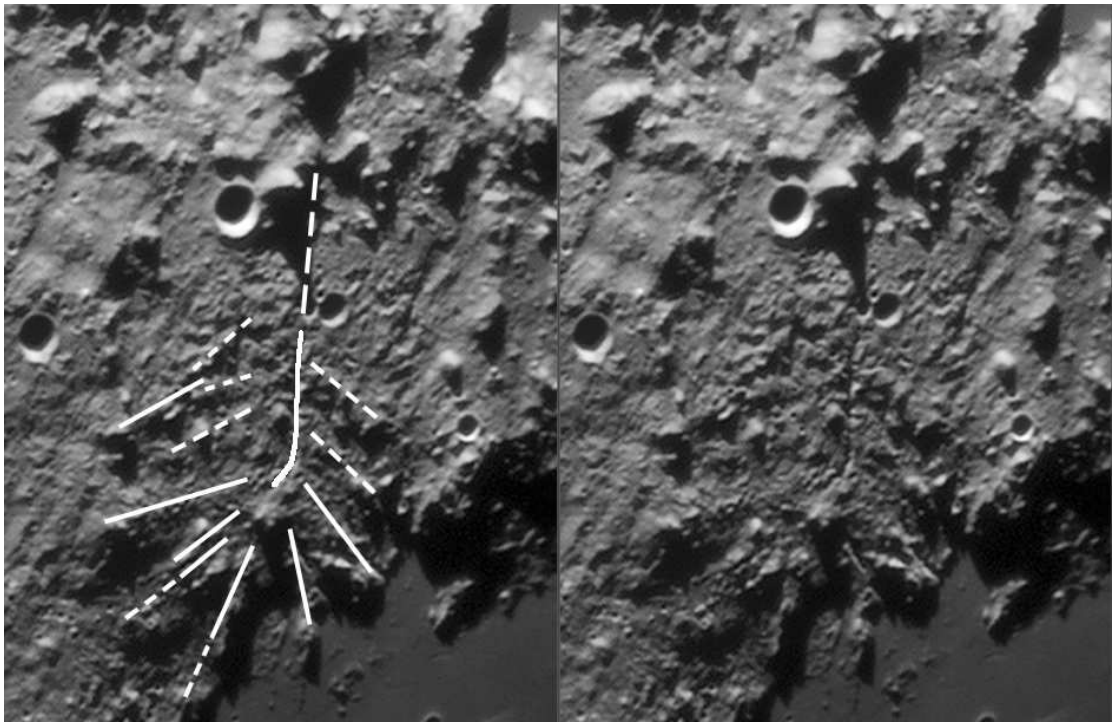

Figure 3. Flow Pattern.

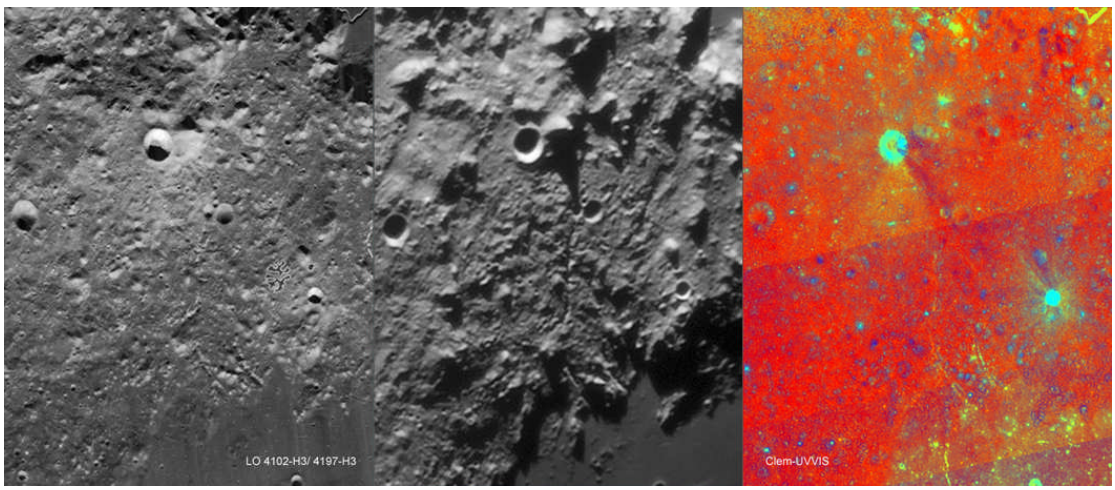

Figure 4. Comparison with Lunar Orbiter image (mosaic of 4-102-H3&4-197-H3) and Clementine colour ratio view.

surroundings. (This is an example of how useful low angle lighting can be in amateur images, showing us things that even much higher resolution spacecraft images can not. With the grazing light from a lower sun angle relatively subtle features become much more noticeable.)

Perhaps the radiating ejecta originated as a huge elongated splash of debris, being ejected up and outwards so it wasn't so much of a flow as a splat as it landed, compared to the larger mounded flow beyond it (Fig. 5) which would have had little or no upward trajectory and so stayed more homogenous as the flow came to rest.This might help explain the central crevice, perhaps the impact of such a large amount of debris would be sufficient to weaken and stress the surface so that when subsequent stresses occurred, perhaps from the cooling of the Imbrium or other lavas in the vicinity, the crevice opened up along the length of the impact. Alternatively the crevice might not be related to the ejecta pattern at all, it could be a coincidental alignment, although the apparent symmetry of the shallow radiating fingers either side of it would seem to argue against this. Further to the south-east the crevice can be seen to continue into the mare manifesting as a line of hills that further develops into a ridge, part of Dorsum Buckland (Fig. 2).

Yet more speculation

The following speculates about the Haemus Mountains beyond the second flow front, which are roughly in alignment with the two apparent flows.

It seems fairly certain that these mountains were formed at the same time as the flows of debris by the Imbrium impact. This is a bit of a long shot but there may be signs of two or three degraded flow fronts among the mountains (Fig. 6).

There seems to be gaps which are relatively clear of debris, which adds to the impression of somewhat separated masses within the flow. Perhaps these degraded fronts would have been ejected with greater velocity than those further back which could explain why they broke up and are now less recognizable. The second one from the back was slower and had the right dynamics to come to rest as a more homogenous mound. The one at the back with the splayed pattern was hurled out and upwards, splashing out on impact. All this is highly speculative of course. This apparent flow pattern raises many questions, ideal for further study and interpretation.

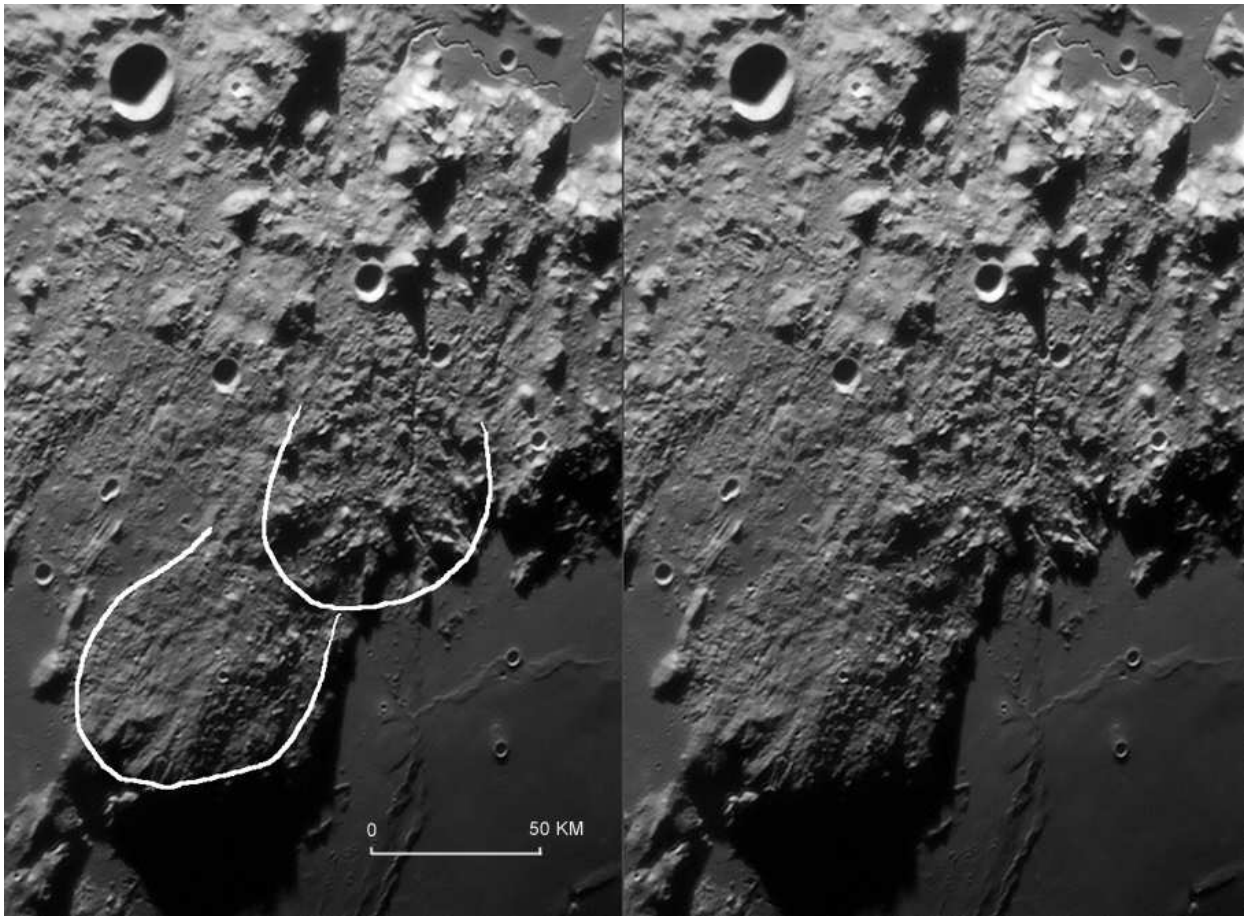

Figure 5. Ejecta flows.

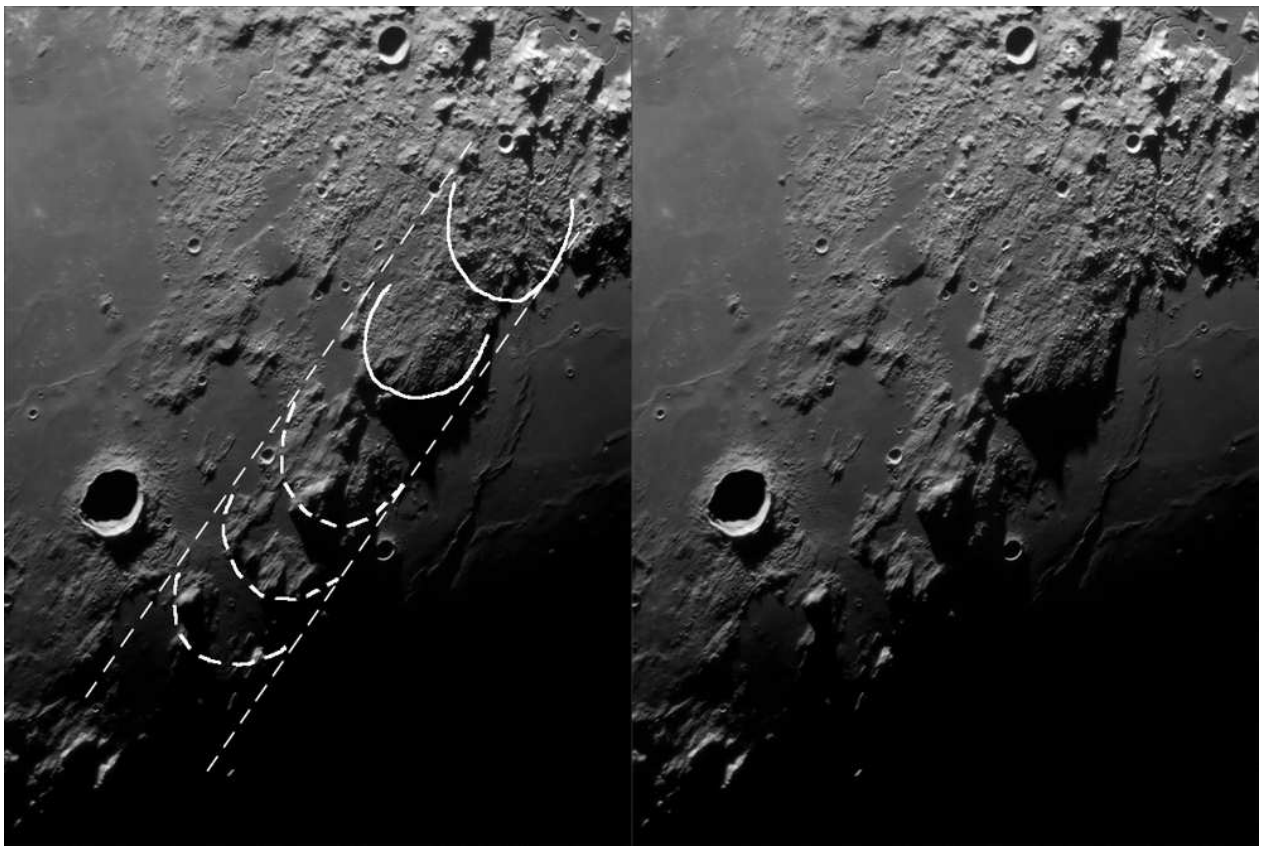

Figure 6. Possible degraded flow fronts.

References

[1] Wood, C., 2009. LPOD: http://lpod.wikispaces.com/August+21,+2009

[2] Carr, M. H. 1966. Geologic Map of the Mare Serenitatis Region of the Moon. U.S. Geological Survey Miscellaneous Geologic Investigations Map I-489 (LAC-42).

[3] The-Moon Wiki. http://the-moon.wikispaces.com/Mare+Imbrium

[4] Masursky, H., Colton, G. W., El-Baz, F., 1978. Apollo over the Moon

http://history.nasa.gov/sp-362/contents.htm

[5] Schultz**,** P. H., 2001. Origin and implications of the Imbrium sculpture**.** Lunar and Planetary Science XXXII.

http://www.lpi.usra.edu/meetings/lpsc2001/pdf/1900.pdf

[6] LPI Lunar Orbiter Photo Gallery.

http://www.lpi.usra.edu/resources/lunarorbiter/mission/?4

[7] USGS Map-a-Planet Explorer: Moon - Clem-UVVIS Ratio Map.

http://www.mapaplanet.org/explorer/moon.html

Using 3-D globes to study the topography of Mare Orientale

By Maurice Collins, Palmerston North, NZ

Email: mauricejscollins@hotmail.com

Website: http://moonscience.yolasite.com/

Introduction

I set out with the goal of wanting to be able to view the Moon in three dimensions like what an astronaut would see on a high-altitude orbit of the Moon. Here is the process I used to create a windows video movie of a rotating 3-D anaglyph Moon-globe from an image of the full-Moon, and also some studies of the Moon using the Kaguya 3-D globe. http://wms.selene.jaxa.jp/3dmoon_e/index_e.html

Creating a 3-D anaglyph globe of the Moon

The procedure is to turn a flat 2-dimensional image of the full Moon into a (half) globe. To do this I used three pieces of software. The first is called the Lunar Terminator Visualisation Tool (LTVT) by Jim Mosher and Henrik Bondo

http://ltvt.wikispaces.com/LTVT.

The second software is Photoshop CS-2, which created the 3-D anaglyph using a procedure outlined on this website named:

"How To Create 3D Anaglyphs in Photoshop" at

http://graphicssoft.about.com/cs/photoshop/ht/3danaglyph.htm

The specific details are repeated in Appendix 1 and in addition to the procedure, the brightness and contrast using "Curves" needs to be adjusted on each image to maximize the 3-D effect. Finally the movie was put together using Windows Movie Maker which comes with all windows operating systems.

How to make the images:

First use your telescope to create a full-disk image of the Moon. Then create a full disk mosaic. I use Microsoft ICE (Image Composition Editor) to create the image mosaic for these images. The next step is to import it into the Lunar Terminator Visualization tool.

Use the option in LTVT "calibrate a user photo" so it is accessible by the software. This is done by setting the images date and time to the reference map on the main screen, loading your image into the "calibrate user photo" screen, then on the main screen map right clicking and setting a reference point (a crater central peak is good to use). Copy this information to the image you are calibrating (there is a button) and select the exact same point on your image as you selected on the map. Only two reference points are needed to

calibrate an image. Then load calibrated photo into the LTVT itself which replaces the map texture with your image. Use the save image button to save the image as a .bmp image. In the "computed geometry" section manually enter a longitude value of 90^0 for the east limb, 0 latitude (or leave it as your images sub-observer latitude as I did), click in the centre of the image to update it (unfortunately there is no button to update it and centre it automatically). Then enter 80 degrees longitude, and save the image. Repeat though 0^0 (centre of the lunar disk) to -90^0 or you can go slightly beyond the western limb also if you wish to go beyond the terminator if it lies on the western limb. The aim is to rotate the globe by about 10^0 of longitude each time. I chose this amount of separation so as to give a very marked 3-D effect. When choosing less the globe of the moon seems flat and not spherical. The reader can adjust this if the effect does not look right to their eyes.

This will build up a set of images to use in creating the 3-D effect. Using Photoshop (or you favorite image processing package), open the 90° image, and the 80° image. Start working from the 90° image and go through the anaglyph procedure on the website or appendix 1. It helps at this stage to record a Photoshop "action" as you go. This remembers your procedure and records it to play back to process the next images, saving a lot of work. You will then only have to do a couple steps manually each time.

Make sure to align the 90° and 80° images so that the limbs match. Do this by reducing the opacity of the two images mid-way through the process. The action will fail at the copy of the 80 image so do this manually each time, then align the two images and then carry on the action from the step that involved moving the layers to the correct positions.

Now save the 90° image as the 3-D anaglyph. Close it. Using the 80° image now, open the 70° image. Apply the same procedure to the 80° image and open the 70 degree image for the next step and so on. If you wish to move in latitude under 3-D you may need to make an addition pair of images of the longitude you select with the same latitude, as it doesn't work using the next image as above, because they are not horizontal with the eye.

How to make the globe rotate:

Finally when you have made a series of 3-D anaglyphs (like in figure 1), use Windows Movie maker which is found on Windows operating system. Import the still images and assemble them into a Window media video file (.wmv) that will create a rotating Moon globe of your anaglyphs. I used the fade effect between images with an image duration of 4 seconds.

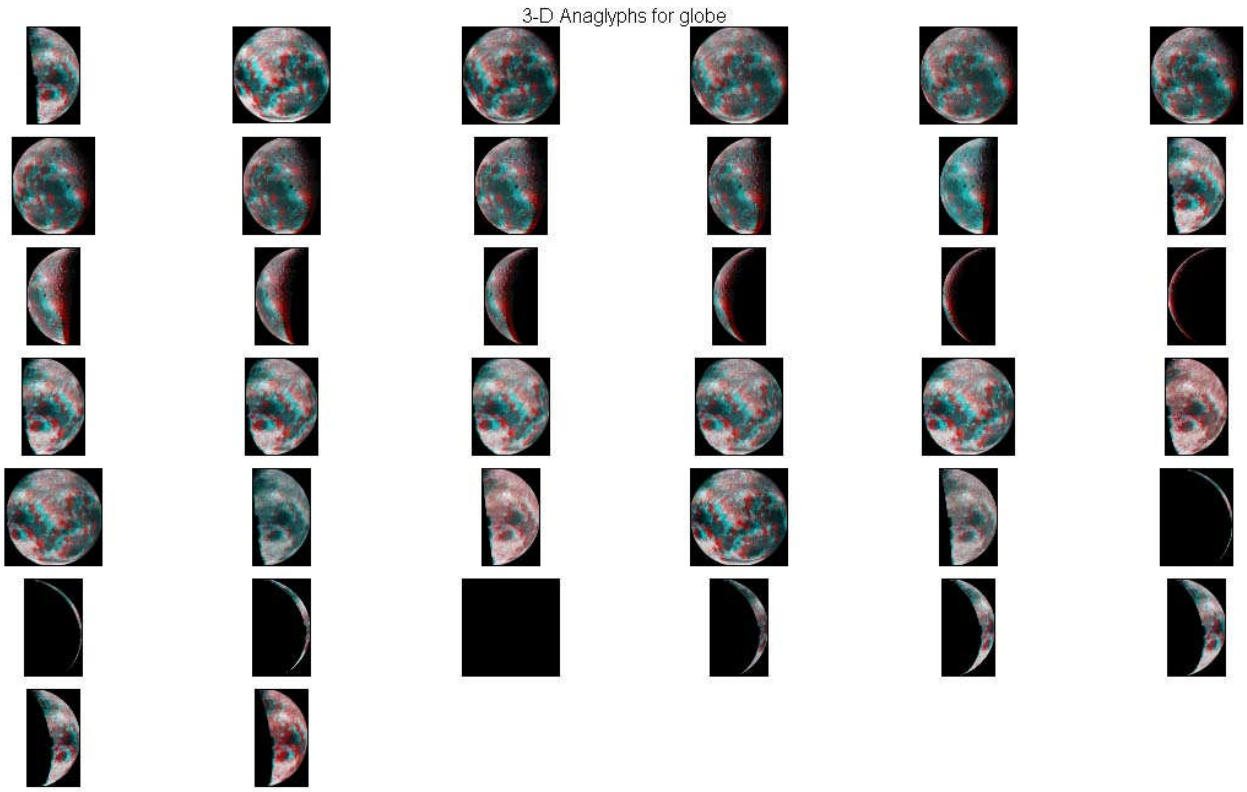

Figure 1 Images from photoshop used to make 3-D anaglyph globe.

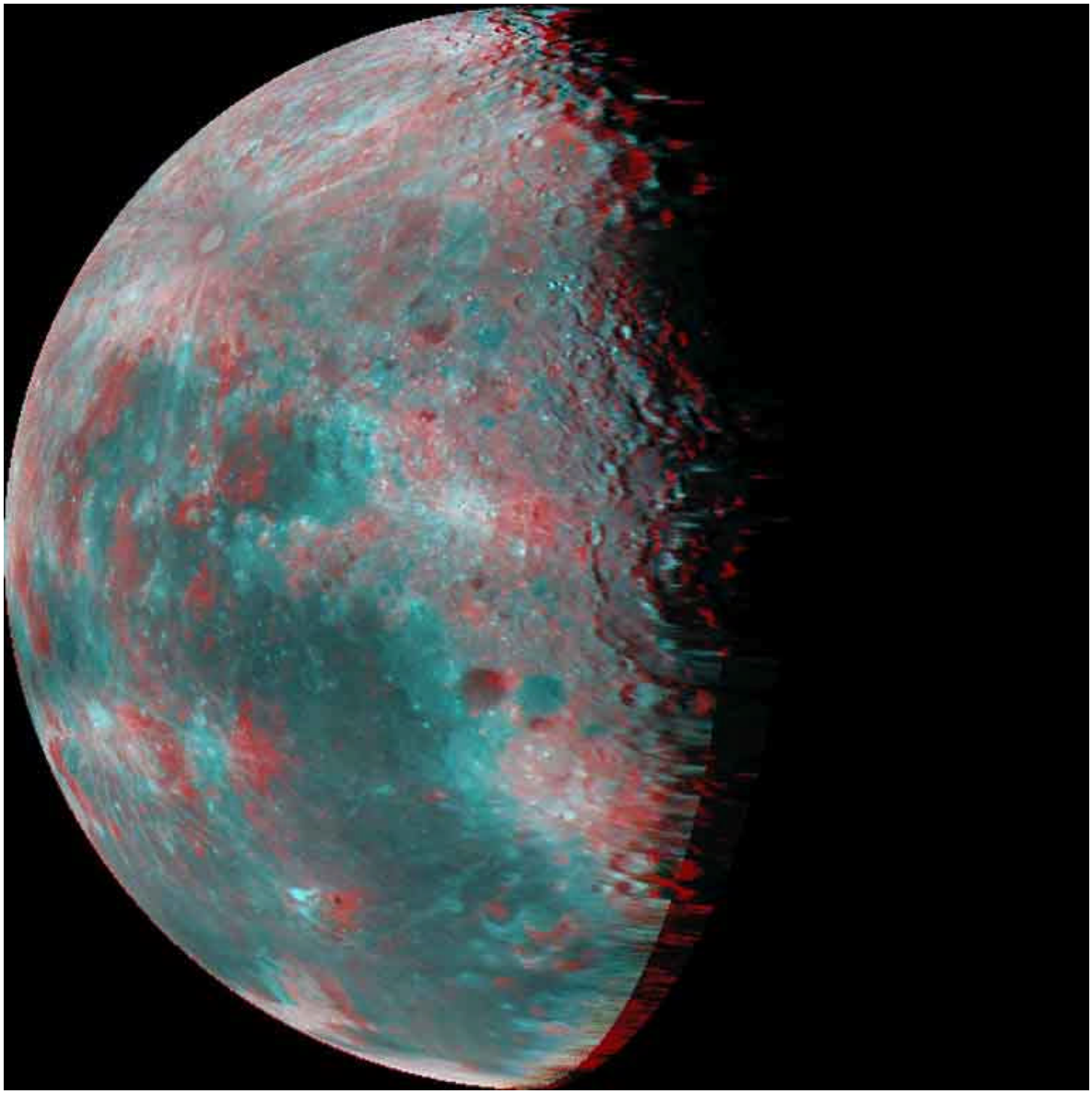

Figure 2: 3-D anaglyph of Mare Orientale. South is at top.

The end product is a 3-D rotating Moon globe. You will of course need red/green 3-D glasses to view it. The globe is available on my website at:

http://moonscience.yolasite.com/3-d-anaglyphs.php

Using the 3-D images for research:

The 3-D anaglyphs can give more insight into the topography of regions of the Moon.

I have used the anaglyph (figure 2) of Mare Orientale to get a better view of the basin rings and radial valleys. Mare Orientale is a relatively young (3.8 billion year) old basin located on the western limb of the Moon. It is a multi-ringed basin formed from an asteroid impact. The rings may be frozen shock waves where the surface has been folded into anticlines by the force of the impact (Baldwin, 1963).

Looking at the surrounding terrain I noticed that radial to the rings are many grooves, especially to the south.

Using the recently released Kaguya 3D globe to investigate these further I counted at least ten valleys radial to the Orientale basin. These groves (figure 4) have two possible causes:

They are secondary impacts (crater chains) from debris ejected during the Orientale basin impact, akin to the Imbrium sculpture surrounding the Imbrium basin.

They are radial fractures where the surface has opened along fault lines caused by the impact.

Further research is needed to determine their ultimate origin.

The anaglyphs show that the area between the grooves are raised ridges (figure 5 and 6), this could indicate piled ejecta, or compression of the surface folding the area between radial fault lines as a radial anticline feature (Baldwin, 1962).

I can also make out three definite rings to the Orientale basin with a possible forth external to that. (Figure 6). There is a section of mountains near Riccioli that could be the D'Alembert mountains as seen by Schroter (Wood, 2003 and Wilkins and Moore, 1961).

Summary

Having a variety of tools for looking at the Moon – 3D anaglyphs and online 3D globes topography globes, Lunar spacecraft imagery and telescopic images - can shed new light on old features and lead to a better understanding of our sister planet, the Moon.

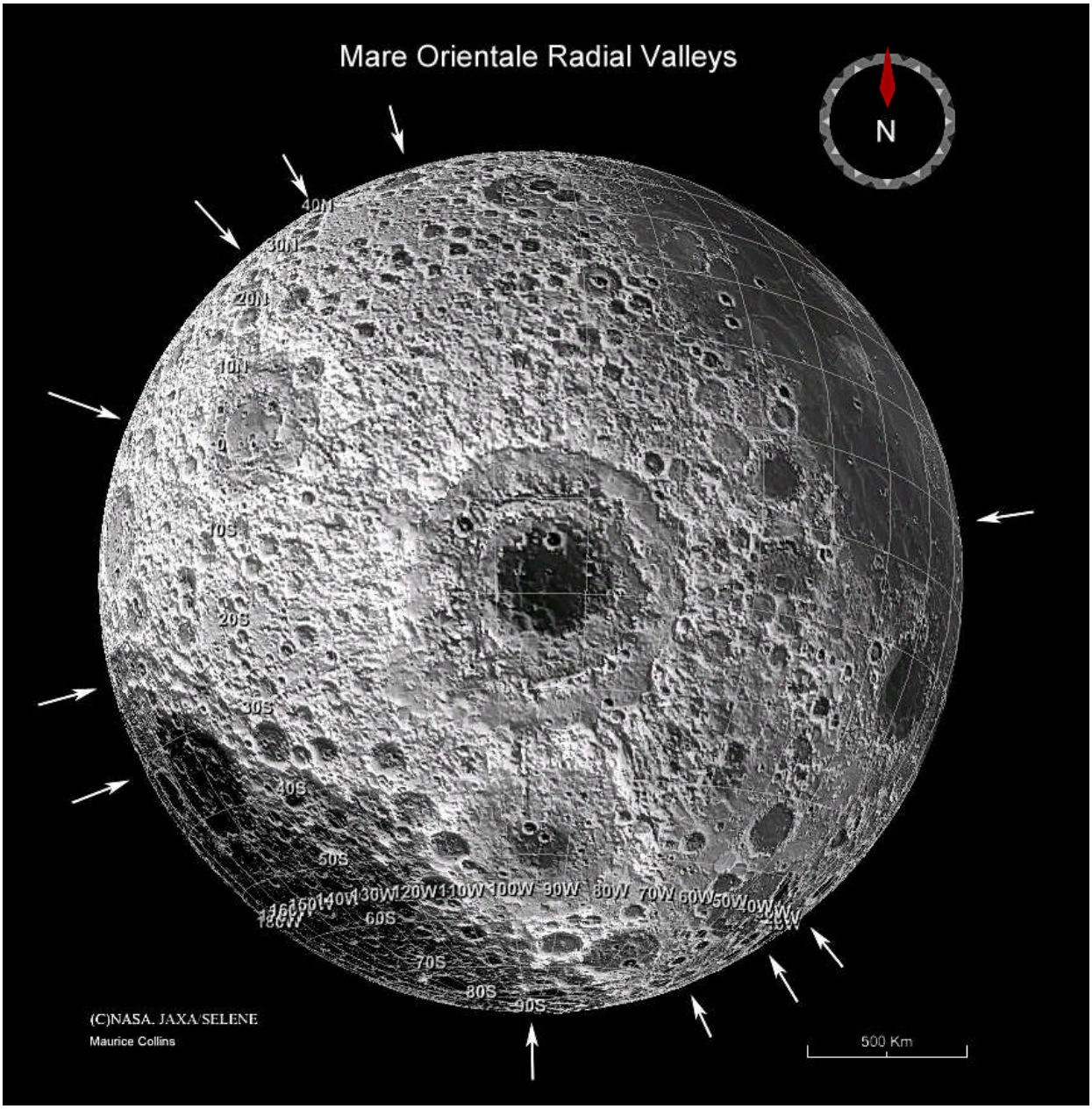

Figure 3: Kaguya 3-D globe image showing the location of the radial valleys surrounding Mare Orientale.

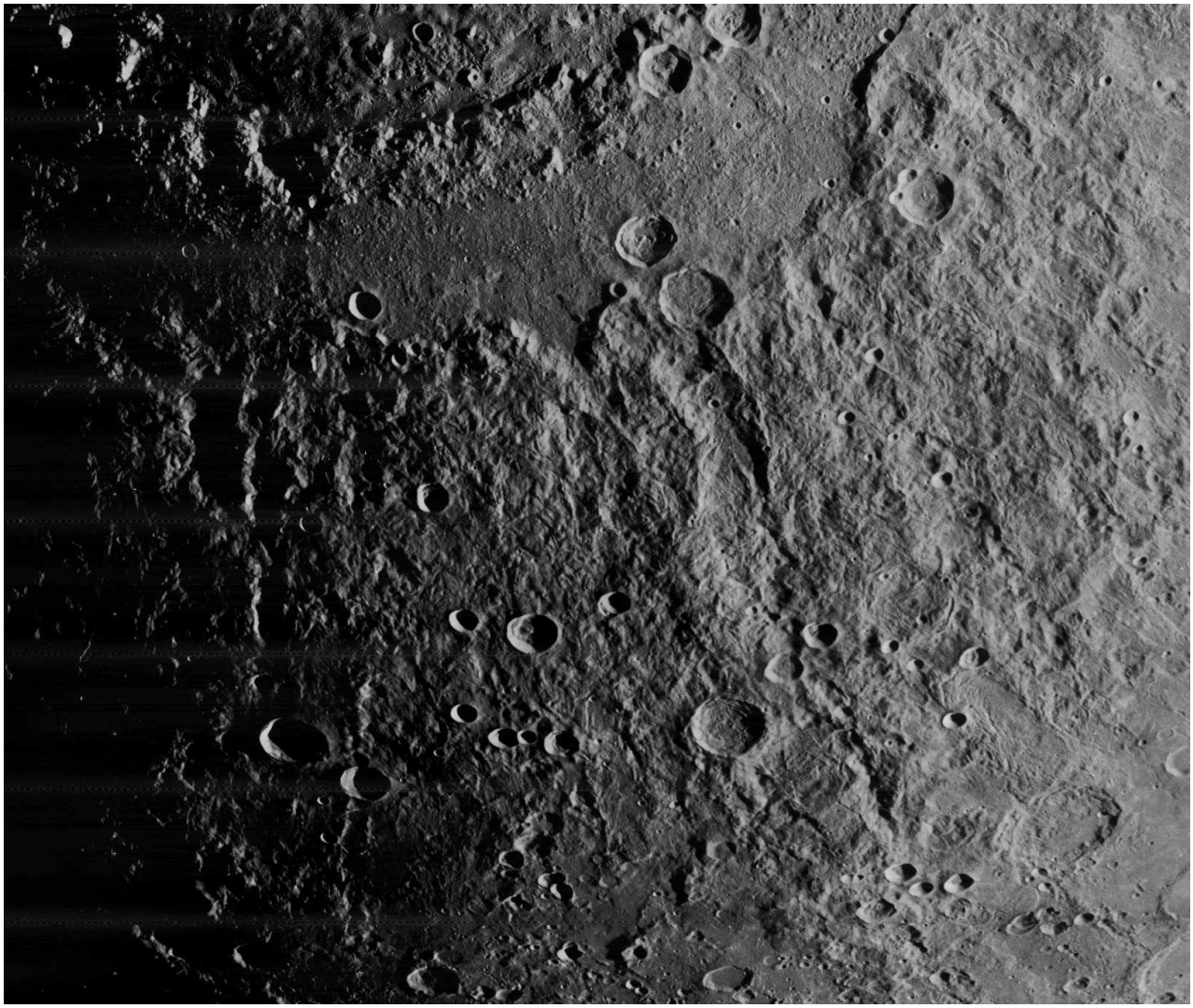

Figure 4 Closeup image from Lunar orbiter image of radial valleys to south of Mare Orientale.

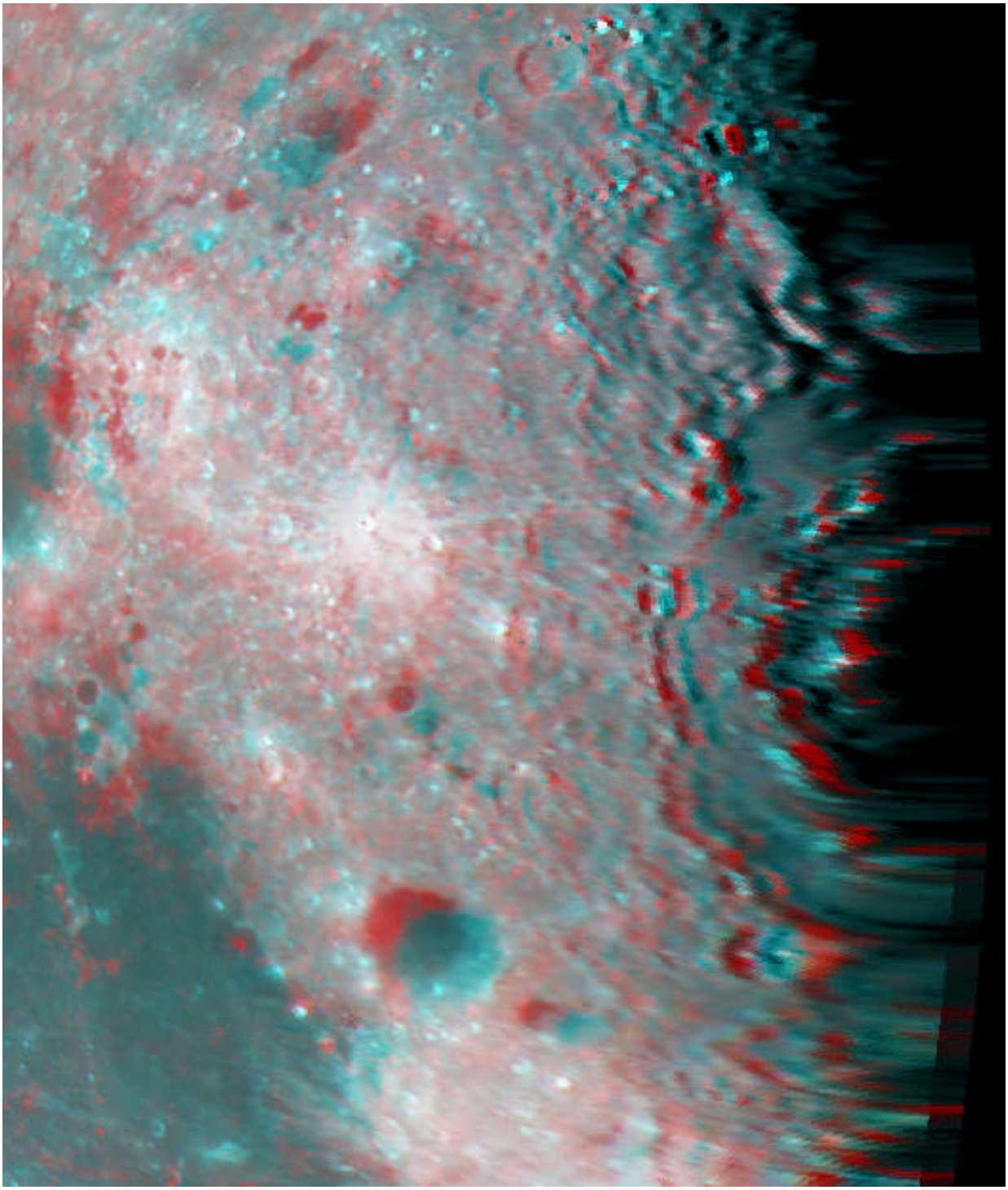

Figure 5 Closeup of the basin and ridge to south (top).

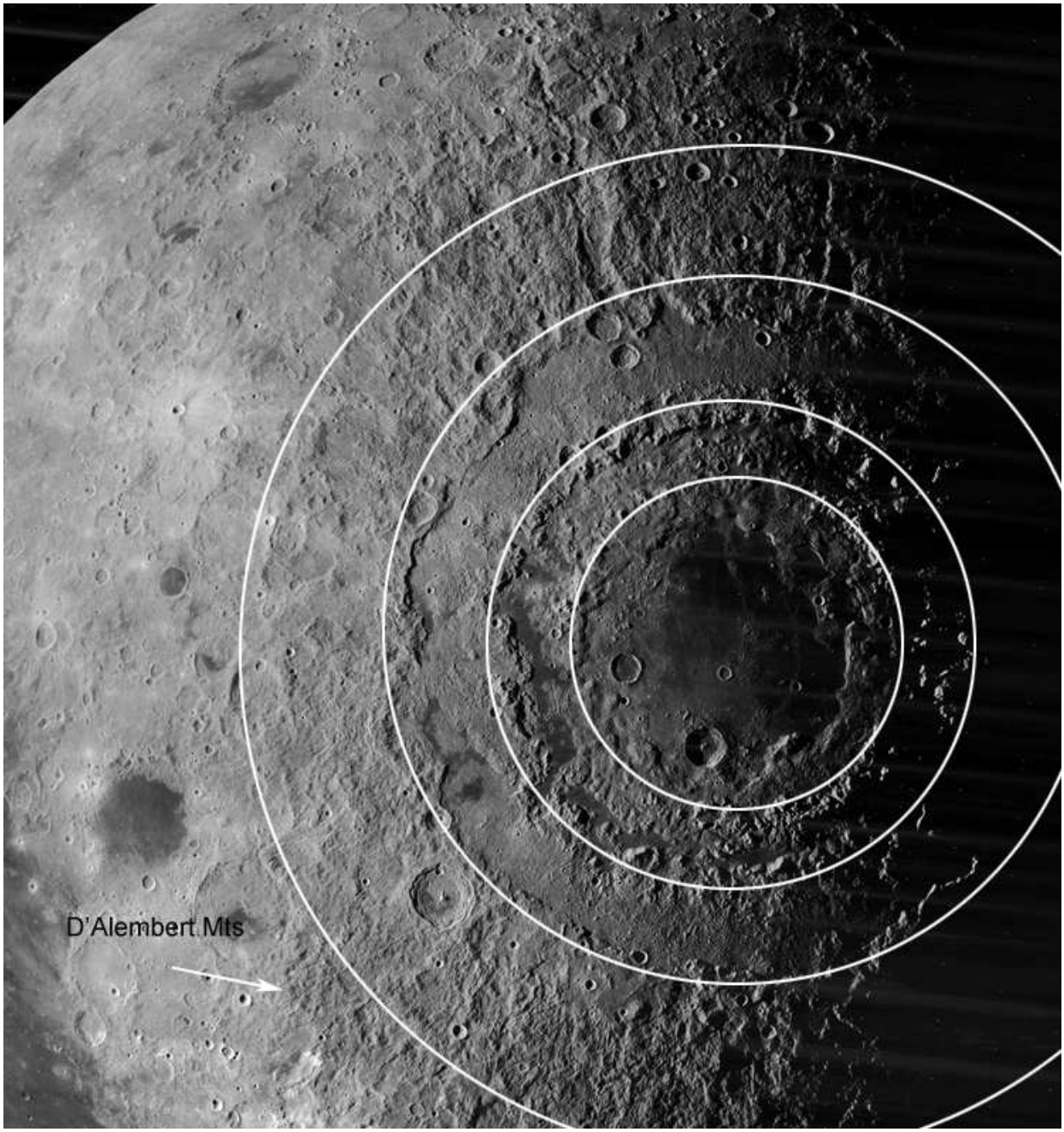

Figure 6 Area approx. corresponding to the anaglyph above showing the Orientale basin rings.

References

[1] Baldwin, Ralph (1962) A Measure of the Moon. Univ of Chicago Press, Chicago USA.

[2] Wilkins, H.P. and Moore (1961) The Moon: A complete description of the surface of the Moon, containing the 300-inch Wilkins Lunar map. Faber and Faber, London.

[3] Wood, Charles. A. (2003) The Modern Moon: A Personal View. Sky Publishing, USA.

Appendix 1

Procedure for creating the anaglyphs

1. Open the photo the left eye would see in Photoshop, this is the one with objects more to the right side of the image.
2. Desaturate if it is a colour image to make it a black and white image:

Image/Adjustments/Desaturate

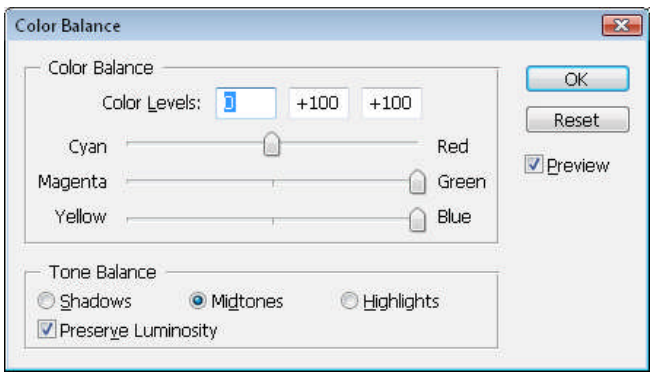

3. Copy (duplicate) the layer twice
4. Set the color balance to:
5. Duplicate this cyan coloured layer
6. Invert this colour to make it Red (Ctrl – I to invert).
7. Open the right eye image and select all and copy (Ctrl-A, Ctrl-C).

8. Paste it over the left eye image below the red layer.

9. Move the cyan layer to the top.

10. Move the background copy to lie between the Cyan at top and Red below it.

11. Delete the main background layer.

12. So the 4 layers are now as follows: The bottom is your right photo. Above it is the red layer. Above it is the left photo and above this is the cyan layer.

13. Now align the images. Turn off the red and cyan layers and adjust the opacity of the left photo to 50%. Move them so they align vertically and have approximate alignment horizontally. Then change the opacity back to 100%. Check the align with the grey scale images also.

14. Turn on the cyan layer and set the mode to screen in the layers tab (from Normal).

15. Merge the cyan layer to the left image. Layers / Merge Down.

16. Turn off the cyan layer and background copy.

17. Turn on the red and right eye image.

18. Change the layer mode to Screen.

19. You may need to adjust the brightness of each layer to look the best.

Archimedes Crater: A spectral study of the south rim "red spot" anomaly

by Rick Evans and Christian Wöhler

Geologic Lunar Research (GLR) group

Abstract

This study uses a spectral mapping technique based on Clementine UVVIS+NIR imagery to assess the composition of Archimedes crater, with special reference to the lunar "red spot" anomaly present on the south rim of the crater. This anomaly has long been suspected to be a pyroclastic deposit. The present study supports that conclusion and confirms the identity of the deposit as being a Group 1 pyroclastic deposit as described by Lucey et al., 1984. Several different calibrations of the Clementine UVVIS+NIR imagery were used and compared. Elemental abundance maps for Al, Ca, Fe, Ti, O, and Mg were generated using a matrix regression based spatial enhancement of Lunar Prospector data as described in Wöhler et al. 2009. The goal was to evaluate the composition of the red spot anomaly.

Introduction

Archimedes is a well known 83 km diameter crater which is situated just northwest of the Appenine Bench formation (ABF), near the eastern border of Mare Imbrium. The stratigraphy of this area has been extensively studied and it is known that the impact which created Archimedes occurred after the Imbrium Basin impact (3.9 to 3.8 Gyr) but before the flooding of the basin by dark mare lavas (3.84 to 3.1 Gyr). The lighter lava plain of the ABF is older than Archimedes and was formed by pre-mare highlands Group volcanism. Archimedes has no rays and its floor is flooded by mare lava. Dark pyroclastic deposits found to be associated with volcanic vents can be found just to the southwest of the crater.

Portions of the rim of Archimedes crater are included in the list of lunar "red spot" features because of strong absorption at ultraviolet wavelengths. The most prominent

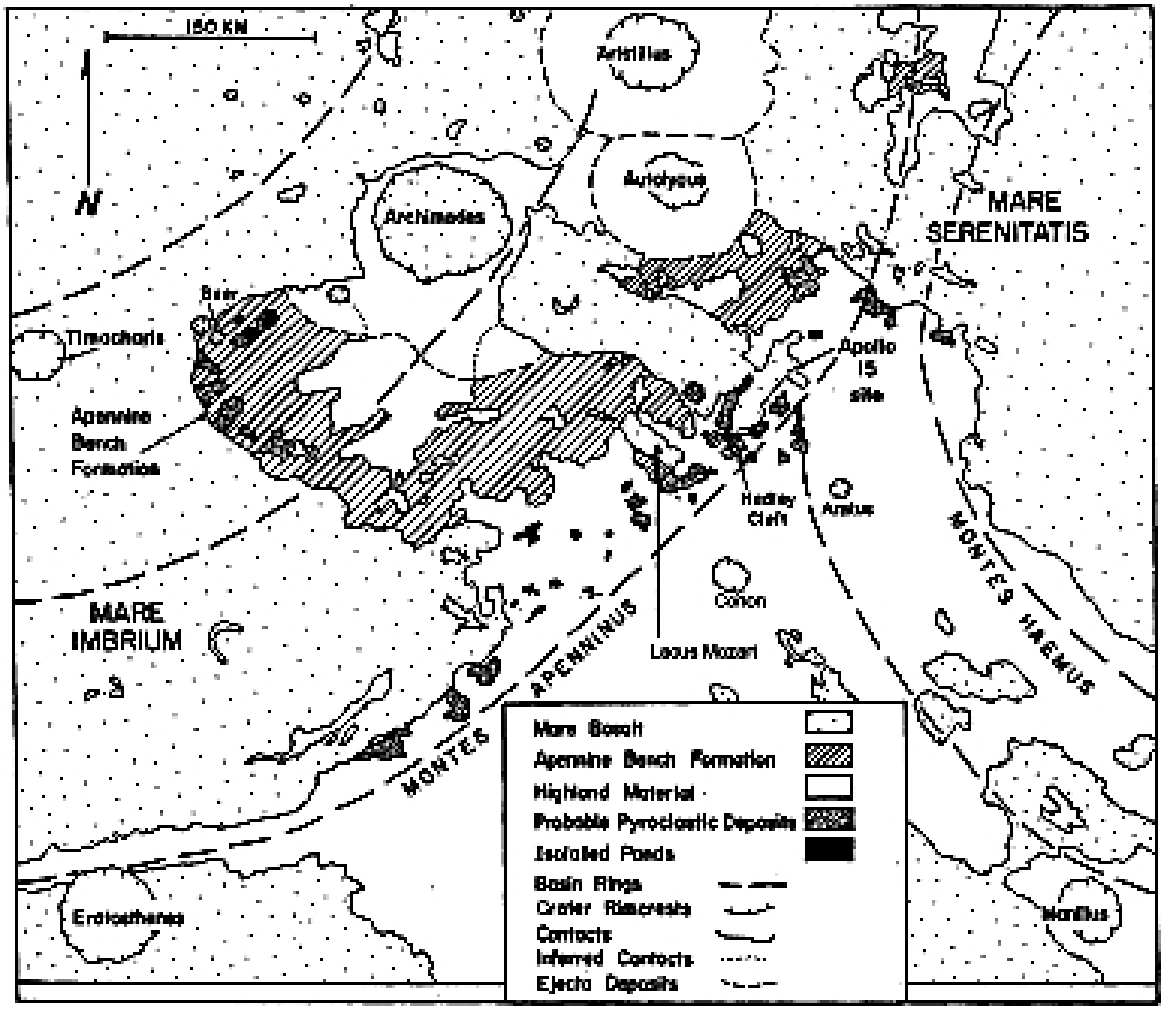

Figure 1a: Archimedes Region

Figure 1a was taken from Blewett and Hawke 2001 and is an adaptation of a figure from Hawke et al. 1979.

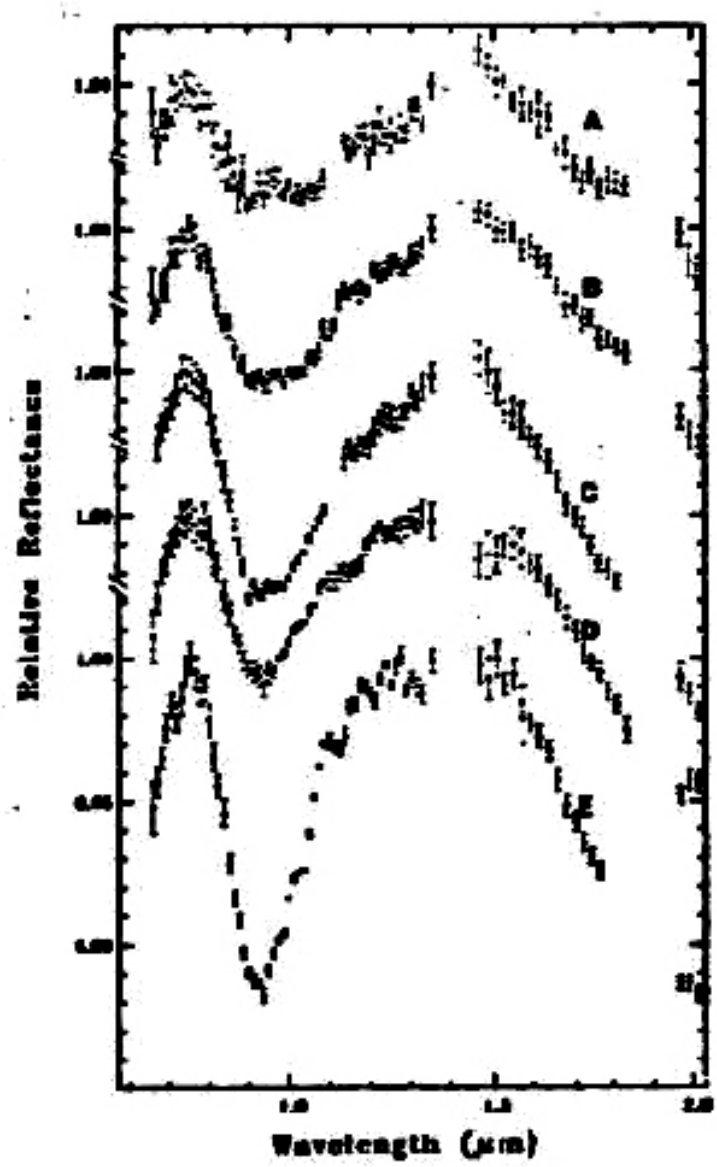

Figure 1b: Earth Based Telescopic Spectrum of Archimedes Region

area is visible below and involves the south rim area and appears dark (low albedo) due to absorption at 415 nm. This area has been found to be very low in Titanium content. Figure 1b shows an Earth based telescopic spectrum of the Archimedes region (Hawke BR and Lucey P, 1984) in which spectrum A is of the Archimedes south rim deposit, B is of Appenine Bench crater 2, C is of the east wall of Archimedes, D is of the wall of Conon, and E is of the Appenine mountains. The complex nature of the trough in the south rim deposit site is clearly visible.

The Optical maturity map (OMAT) of the crater shows low OMAT values for this area of the southern rim and this has been interpreted as being consistent with pyroclastic debris (Hawke et al., 2003). Volcanic vents have been described in the area (Gillis et al., 1999). Numerous other pyroclastic deposits are present along the borders of the Appenine Bench Formation (ABF) and are shown in Figure 1.

The "reddness" of the rim deposits is well visualized in Figure 4 which is a maturation ratio image in which the 750nm/415nm ratio image is assigned to the red channel, the 750nm/950nm ratio image is assigned to the green channel and the 415nm/750nm ratio image is assigned to the blue channel. Dull or darker red rim areas are frequently old areas of gabbroic anorthosite while younger ones are blue. Yellow to orange mare areas are often composed of basalt with a high iron but a low titanium content while bluish mare areas are often composed of basalt with both a high iron and titanium content. The rim deposits in Figure 4, discussed above, have a striking scarlet color.

An important clue to the mineral composition of the rim of Archimedes comes from the FeO wt%. Figure 5 is a Clementine binned color map of FeO wt% and shows that the rim wall is roughly 10 wt% FeO. This would not be consistent with gabbroic anorthosite or anorthositic gabbro which would have much lower iron content. It is more consistent with a medium K Fra Mauro basaltic (M-K FM Basalt) breccia since this Group of highlands rock typically has an iron content of about 9 to 11 wt% and a titanium content of about 2 wt%. The higher iron content within the crater and adjacent to the crater (green) is typical of mare basalt. Figure 5b is a 2000nm/1500 nm image of Archimedes. The brightness of the south rim deposit area in this ratio image favors the presence of some olivine within the overall lithology at this location (Le Mouelic et al., 1999). Some olivine component may also be present in the north rim area.

Methodology and Results

This paper employs the Clementine UVVIS+NIR spectral mapping technique developed and explained in detail in Evans et al. (2009). The technique is used to produce spectral

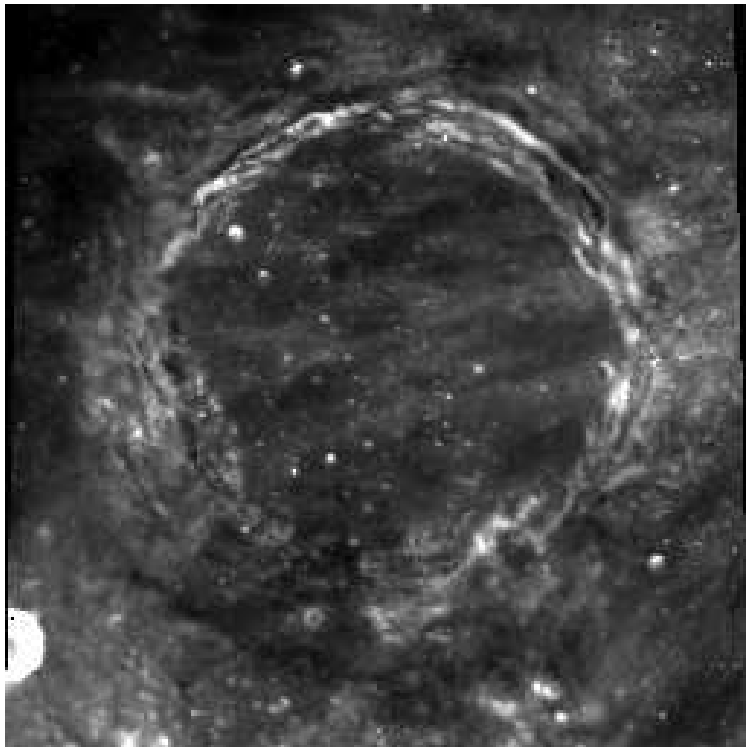

Figure 2: Clementine 415 nm

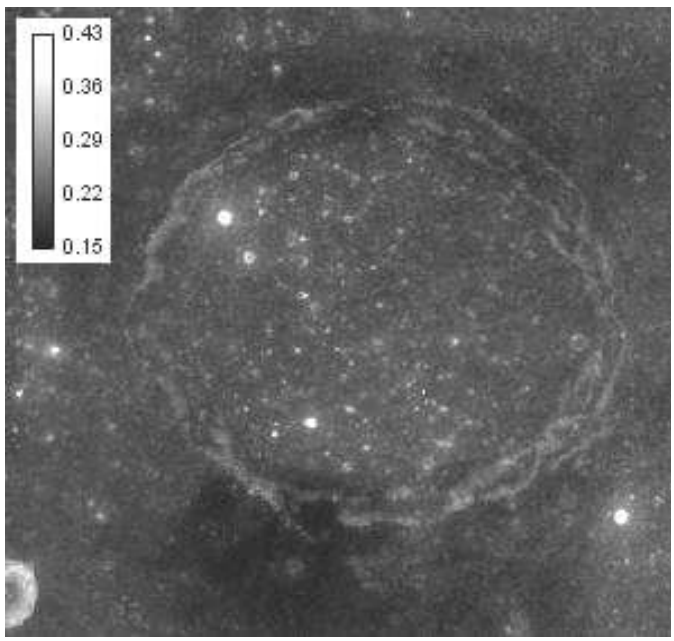

Figure 3: Optical Maturity (OMAT) Map

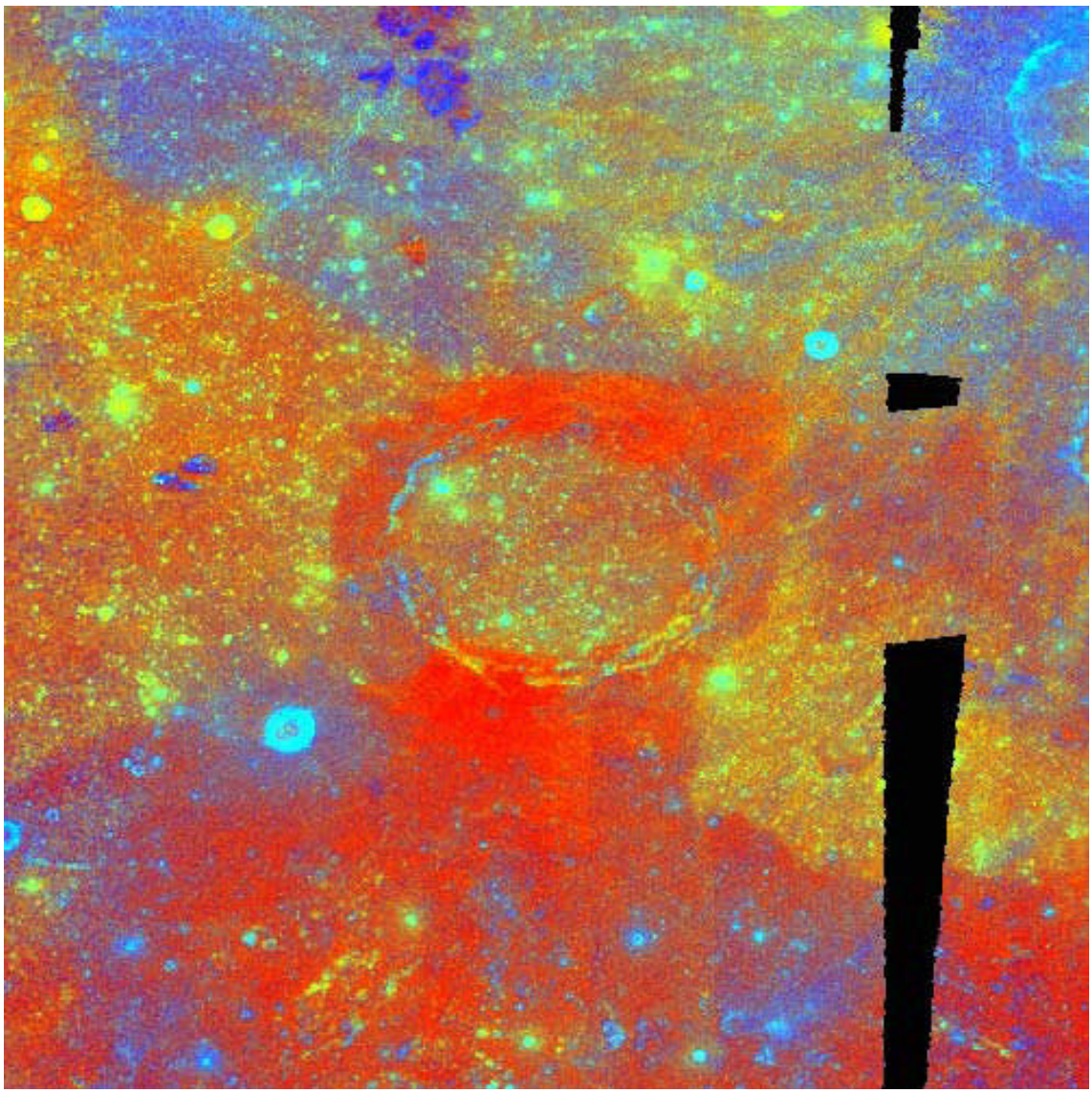

Figure 4: Maturation Image

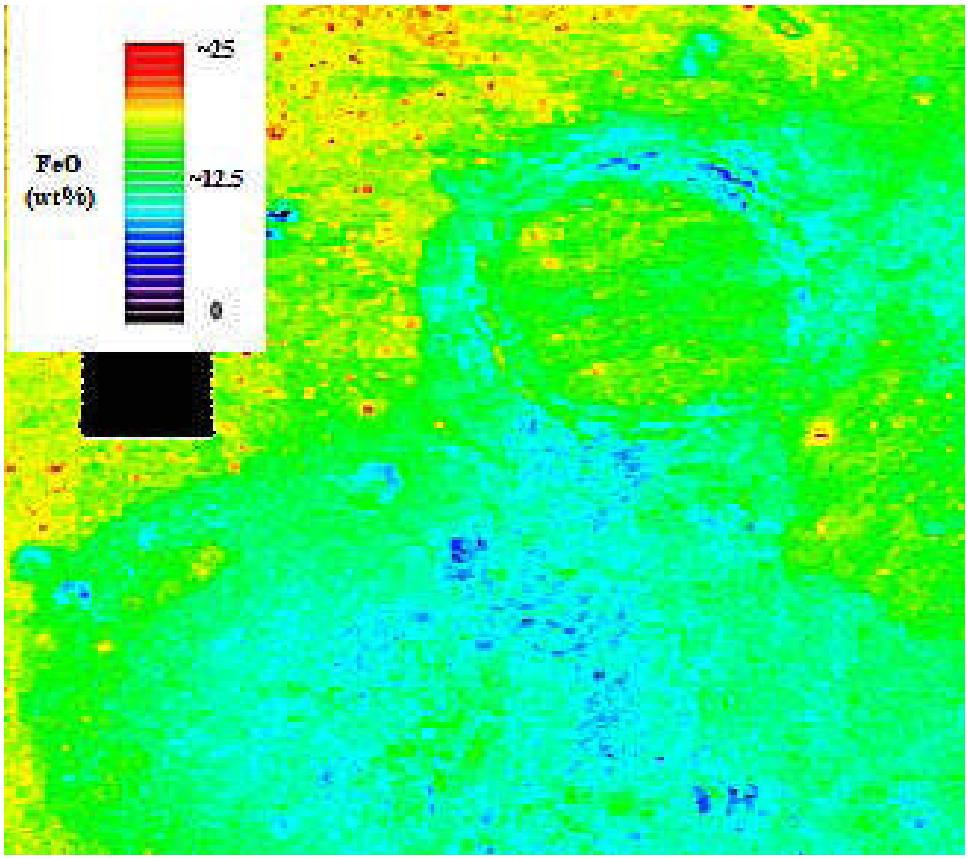

Figure 5a: FeO Map (Clementine binned color)

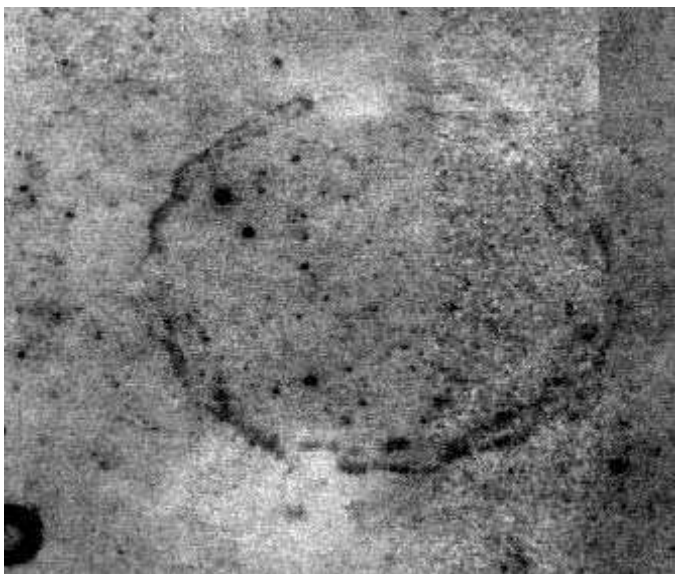

Figure 5b: 2000 nm/1500 nm Ratio Image

maps of the principal spectral mafic absorption features for lunar terrain of interest. It was employed here in an attempt to further discern the minerology of Archimedes. The spectral maps shown in Figure 8a to 8h were produced using this method together with a calibration based on Keck 8 peak spectra as explained below. The original maps were 32 bit tiff. Referring to Figure 8g below, the pyroclastic deposit involving the south rim area is well shown in the FWHM map image, where the average FWHM bandwidth for the deposit area is about 393 nm +/- 25. This is significantly more than the bandwidth for the adjacent rim breccia. Interestingly, the general area of the deposit is shown to have a band center wavelength (bcw) of about 940 nm with a shallow trough depth of about 3.7 to 4.0%. This would be consistent with the Group 1 pyroclastic deposit described by Lucey et al., 1984. A spline interpolated Clementine UVVIS+NIR spectrum of this deposit using the standard USGS calibration is shown in Figure 6a. It is interesting to compare this spectrum with that of an Earth based telescope shown in Figure 1b. The remainder of the crater rim is largely composed of a gabbroic material with a band center at 984 nm and a band depth of about 10% but also having some olivine component as would be expected from MKLF basalt. The most gabbroic area appears to be the north rim. Maps of areas having band centers above 1000 nm area present within the crater interior (floor) where they represent mare basalt and similarly adjacent to the crater rim. When comparing spectral, it is important to refer to the pixel value scale and not to rely on comparison of light and dark areas within a given map type.

Clementine UVVIS+NIR Calibration Issues:

It is well known that thermal instability in the Clementine NIR cameras causes some calibration problems for NIR wavelength images. As a result, Clementine UVVIS+NIR images with the standard USGS calibration do not conform perfectly to spectra taken with Earth based telescopes. In an attempt to correct this problem, Lucey derived a calibration of Clementine UVVIS+NIR imagery based on Earth based telescopic images of the Aristarchus Plateau (see http://astrogeology.usgs.gov/Projects/ClementineNIR/). Spectra obtained using the standard USGS calibration of the Archimedes crater south rim deposit is shown in Figure 6b and the Lucey calibration of the same area is shown in Figure 6c. In this paper, we derive a calibration based on Keck spectra of eight central crater peaks. The result of applying this calibration to the south rim deposit of Archimedes crater is shown in Figure 6d. Overall, the Keck eight peak calibration appears to be a good compromise and to give reasonable results for the absorption trough morphology near 1000 nm. However, the three calibrations do not produce radically different results.

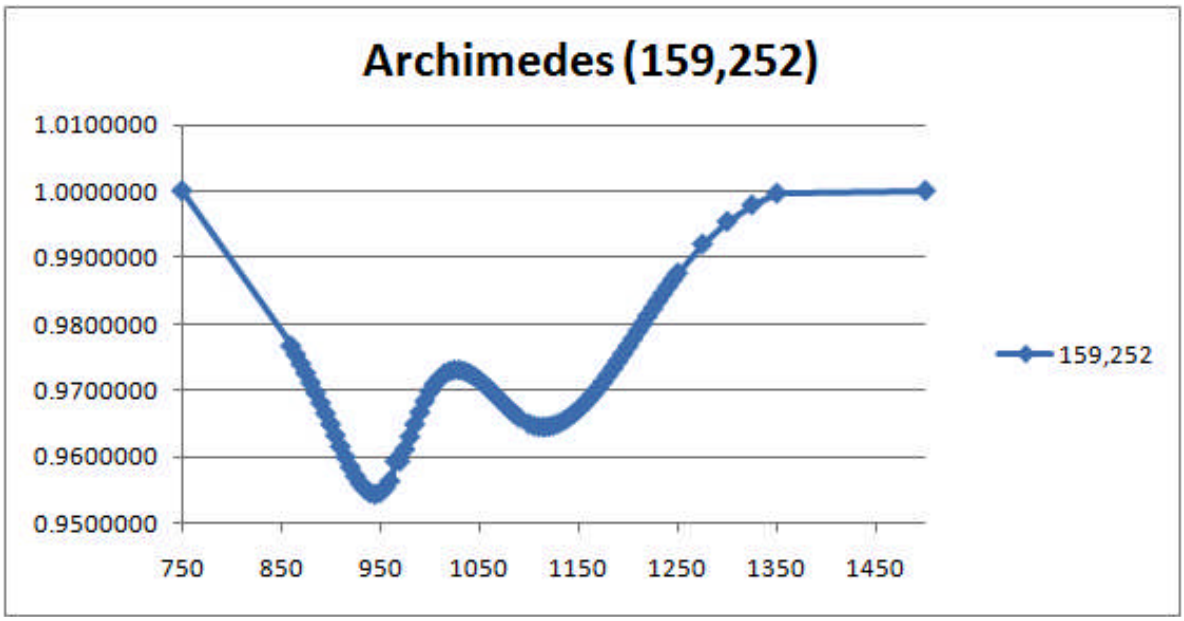

Figure 6a: Cubic Spline Interpolated Spectra of South Rim Anomaly (Continuum Divided), standard USGS calibration

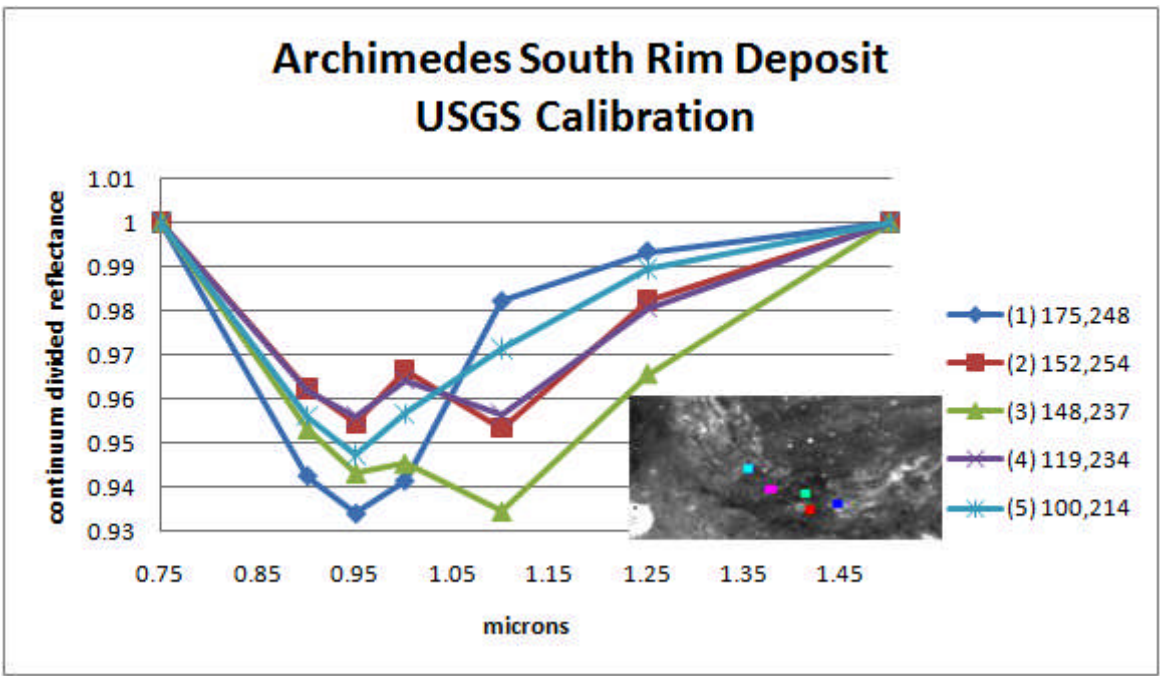

Figure 6b: Non-Interpolated spectra of Multiple Loci within the Red Spot Area (Continuum Divided, Normalized to 1.0 at 750 nm)

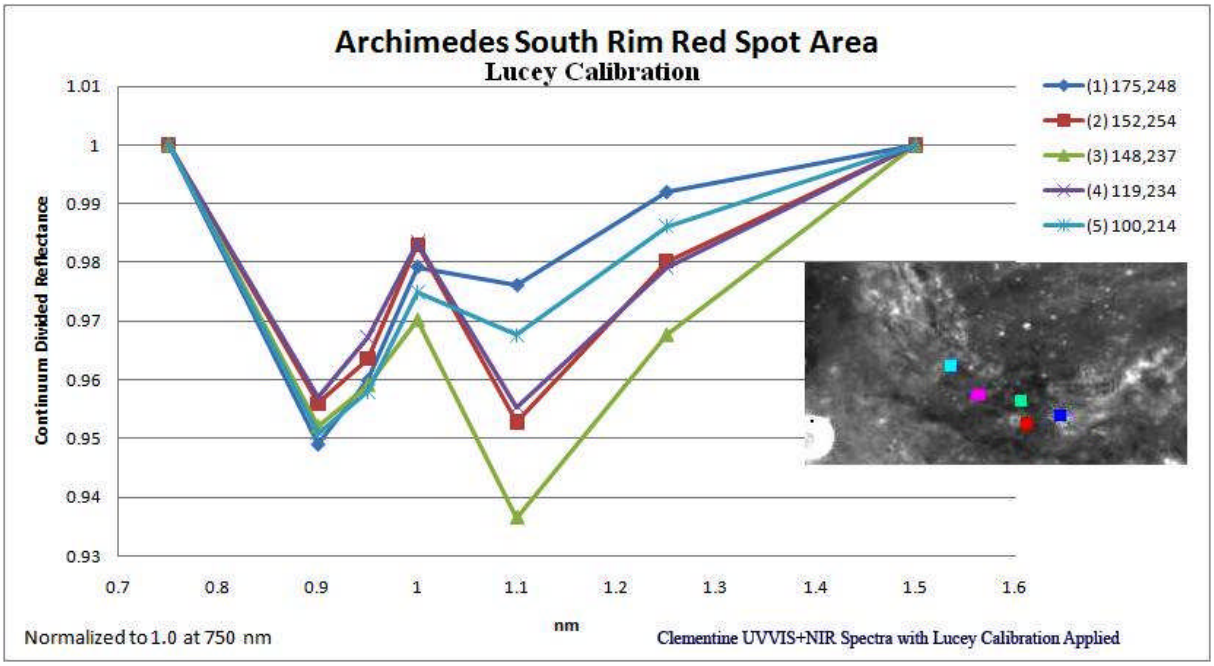

Figure 6c: Lucey Calibration

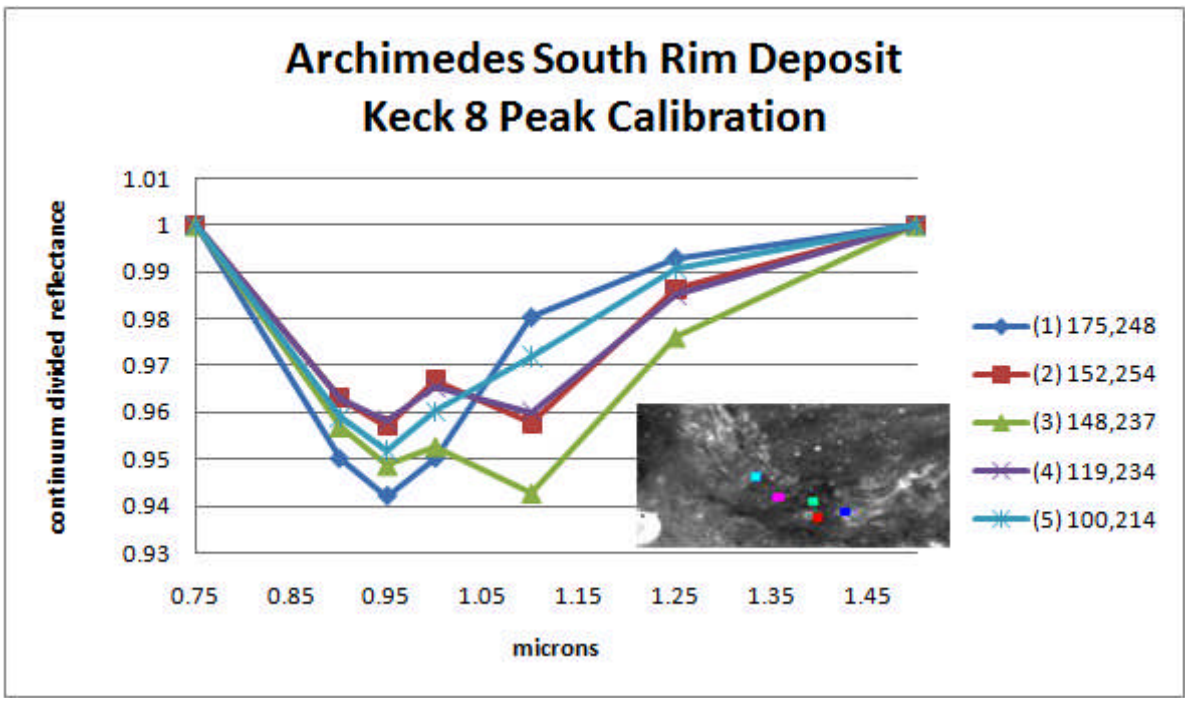

Figure 6d: Keck 8 Peak Calibration

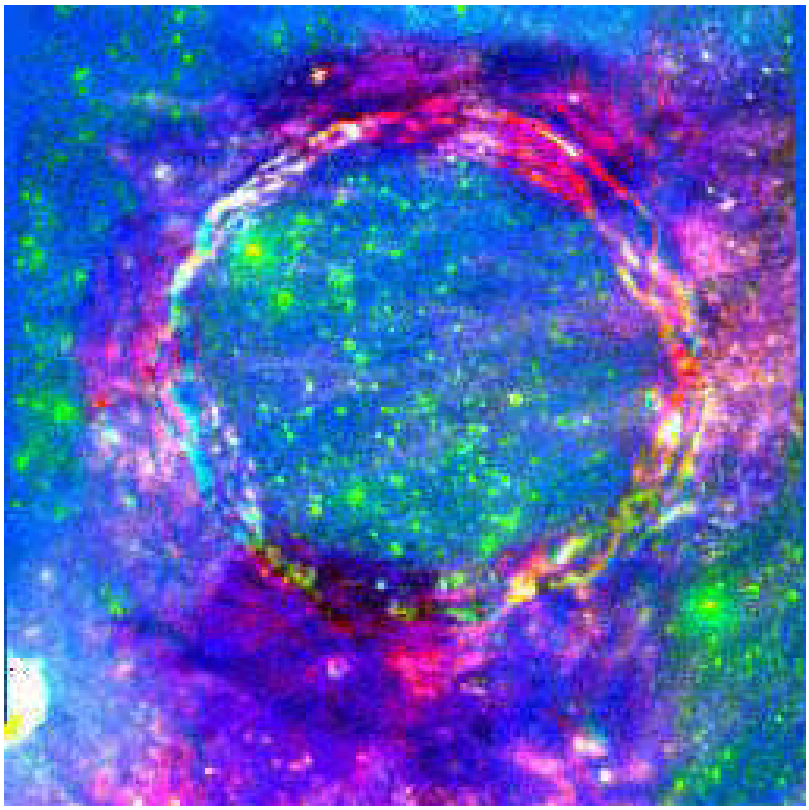

Figure 7: Principal Component Image (UVVIS), USGS calibration

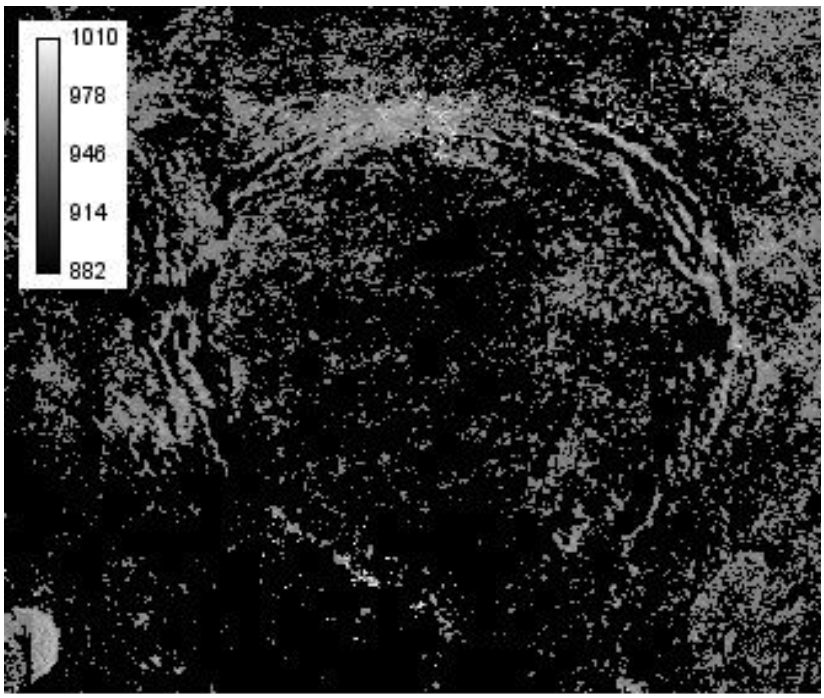

Figure 8a: Keck 8 peak calibration, Clinopyroxene bcw map

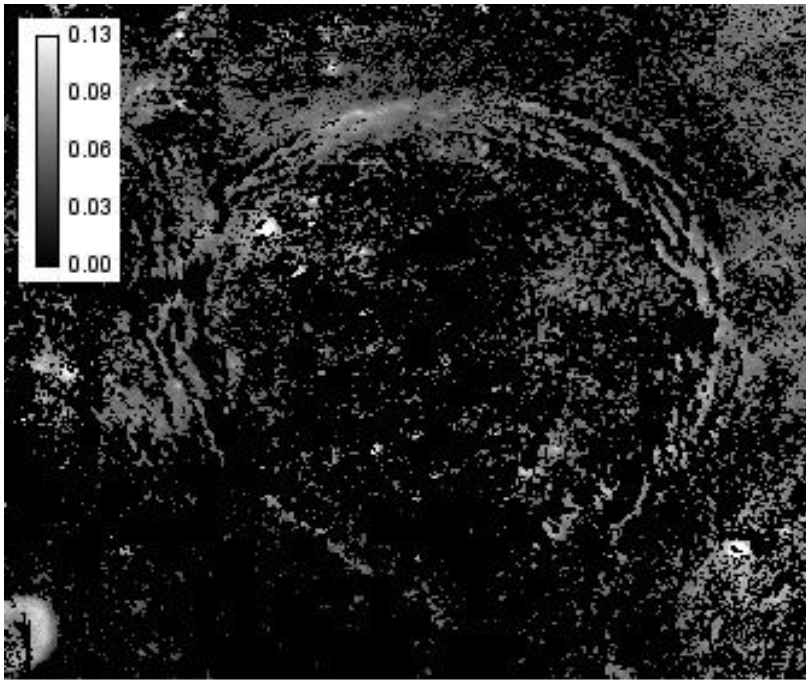

Figure 8b: Keck 8 peak calibration, Clinopyroxene band depth map

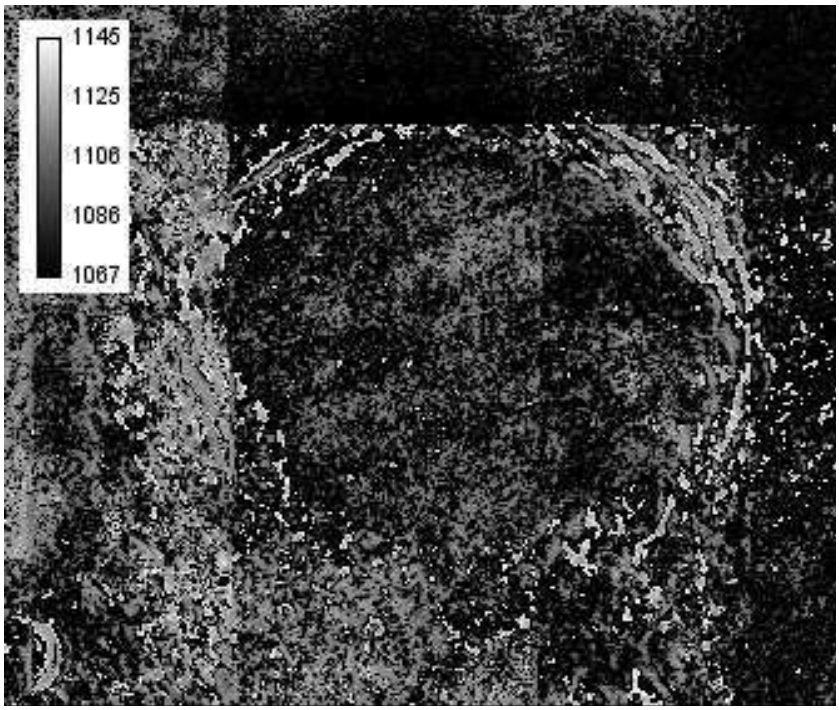

Figure 8c: Keck 8 peak calibration, "Olivine" bcw map

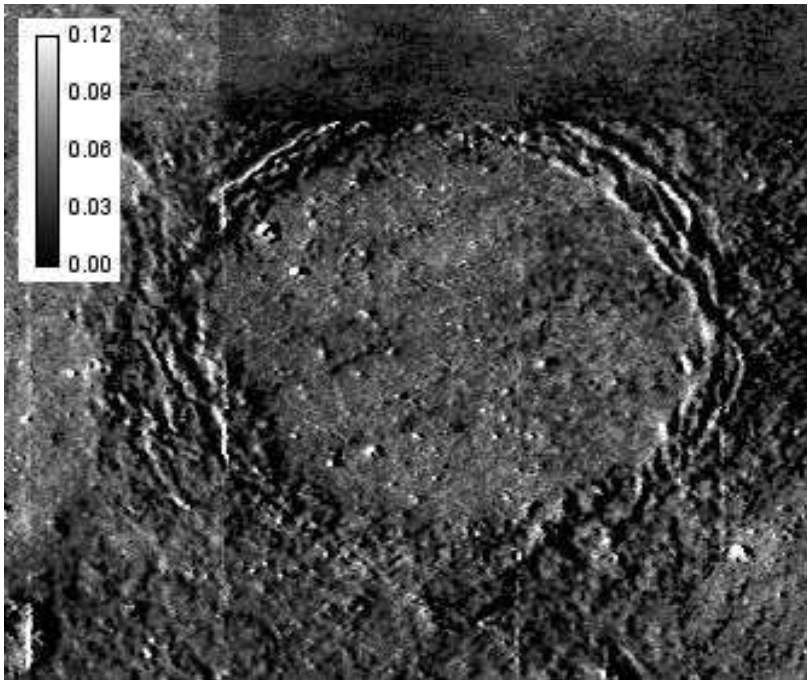

Figure 8d: Keck 8 peak calibration, "Olivine" band depth map

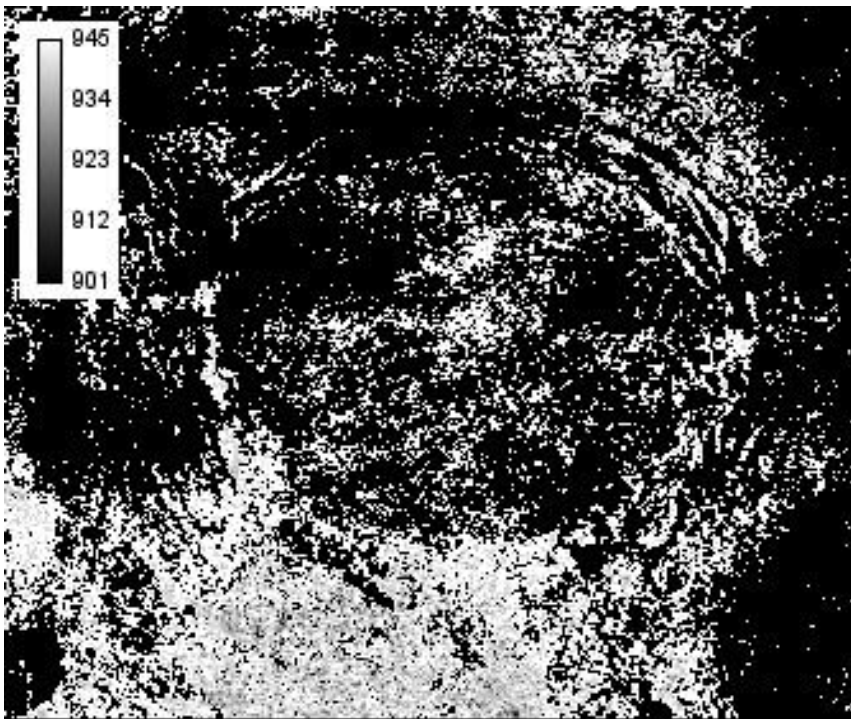

Figure 8e: Keck 8 peak calibration, orthopyroxene bcw map

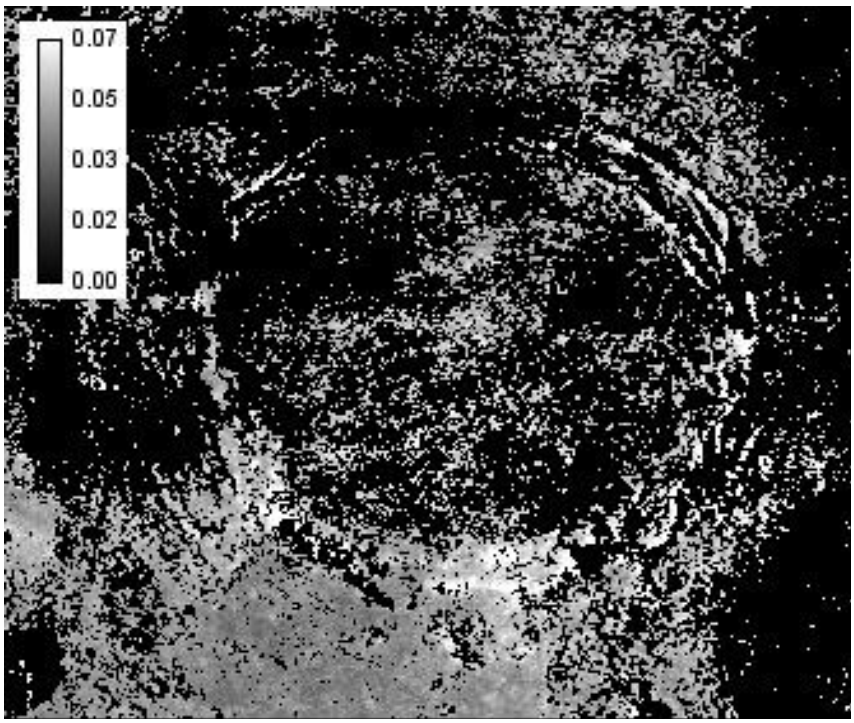

Figure 8f: Keck 8 peak calibration, orthopyroxene band depth map

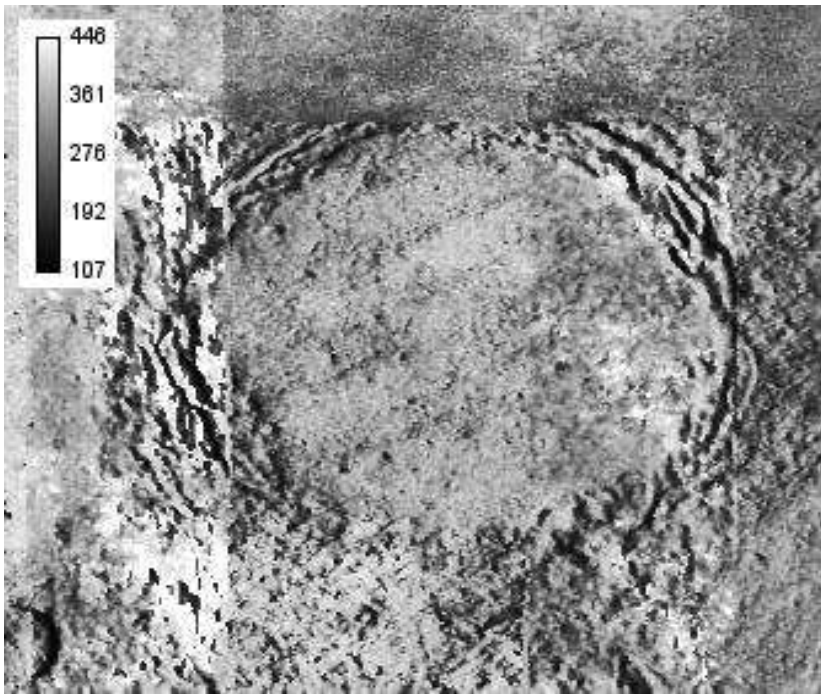

Figure 8g: Keck 8 peak calibration, FWHM map

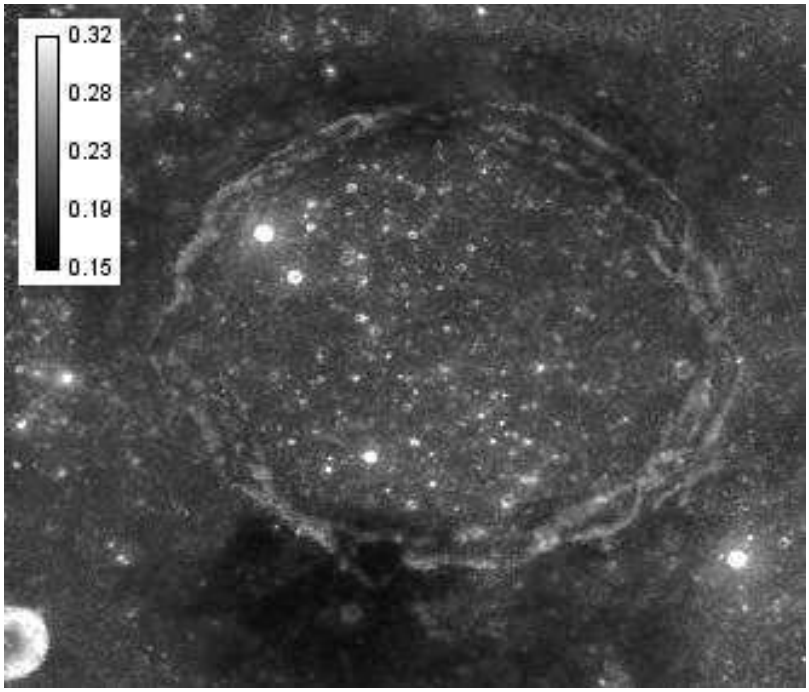

Figure 8h: Keck 8 peak calibration, OMAT map

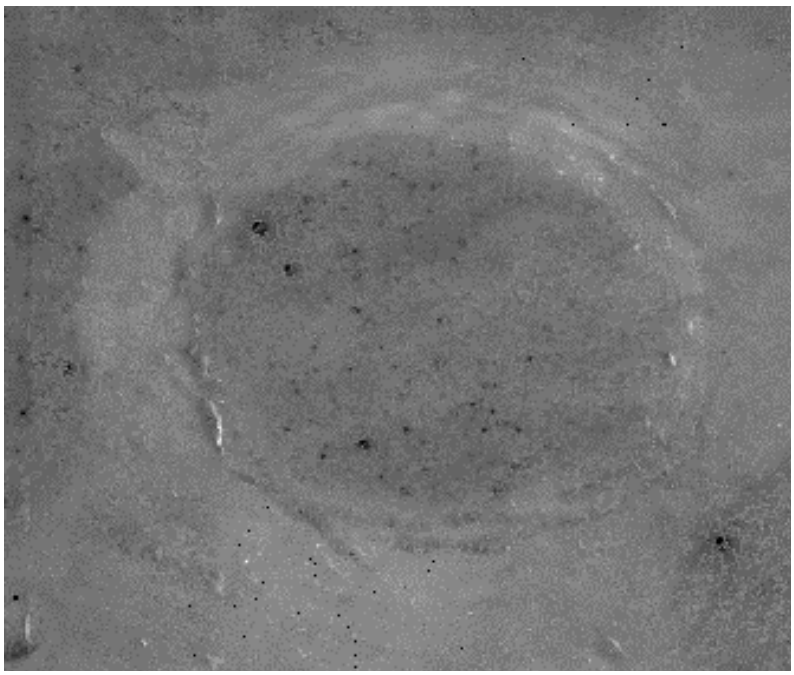

Figure 9a: aluminum abundance

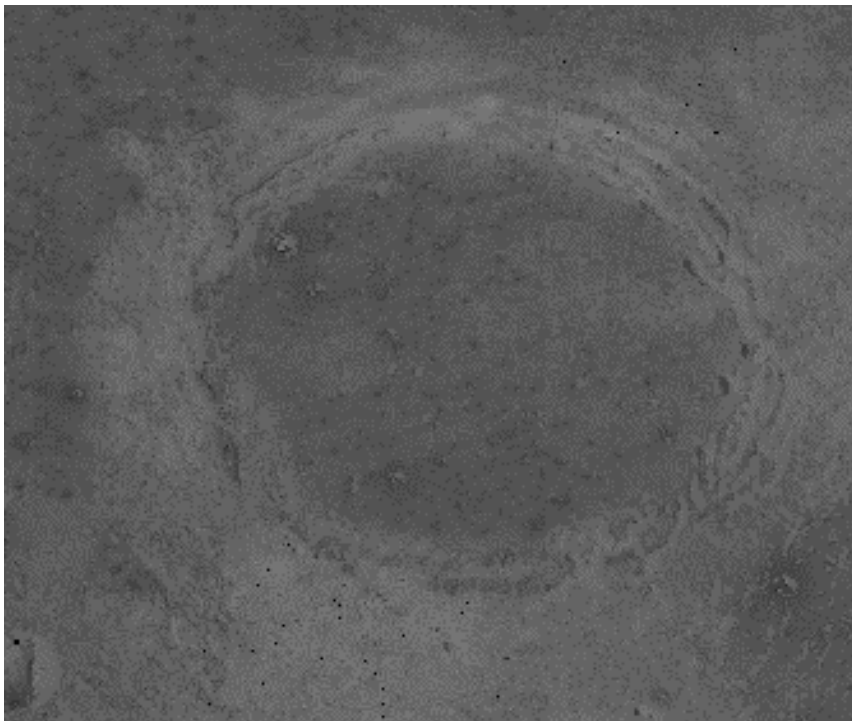

Figure 9b: calcium abundance

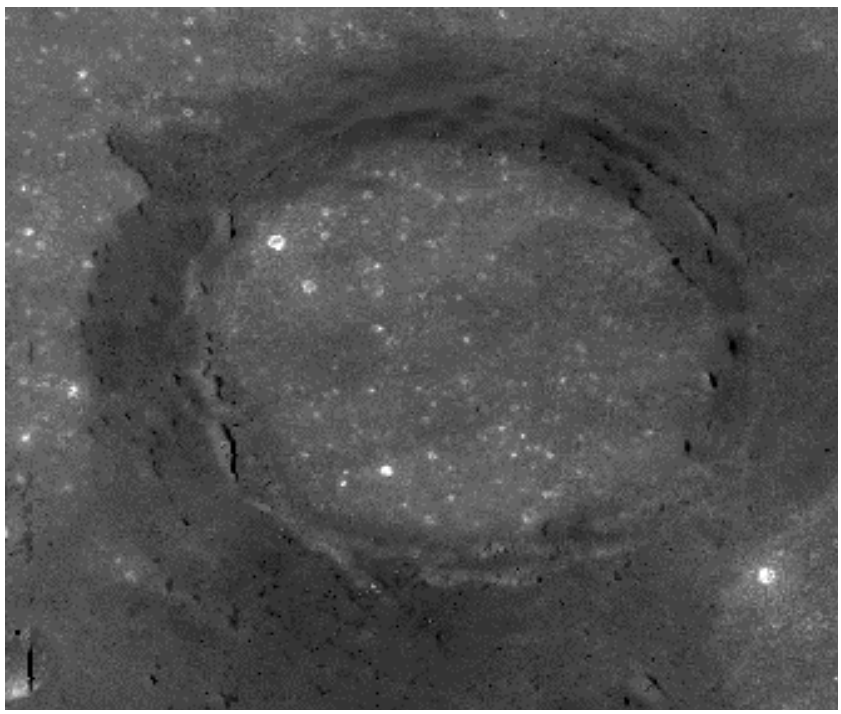

Figure 9c: Iron abundance

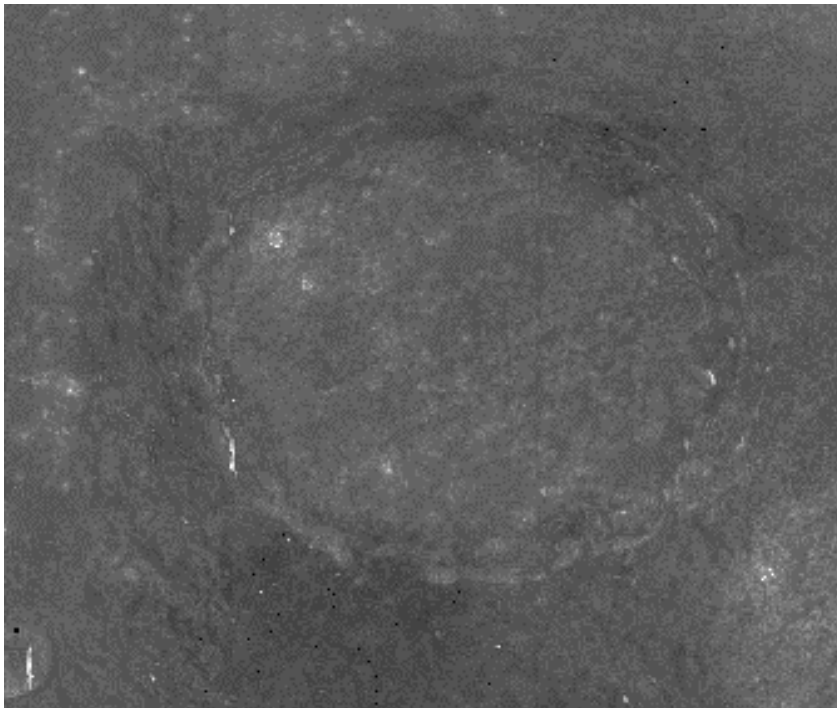

Figure 9d: Magnesium abundance

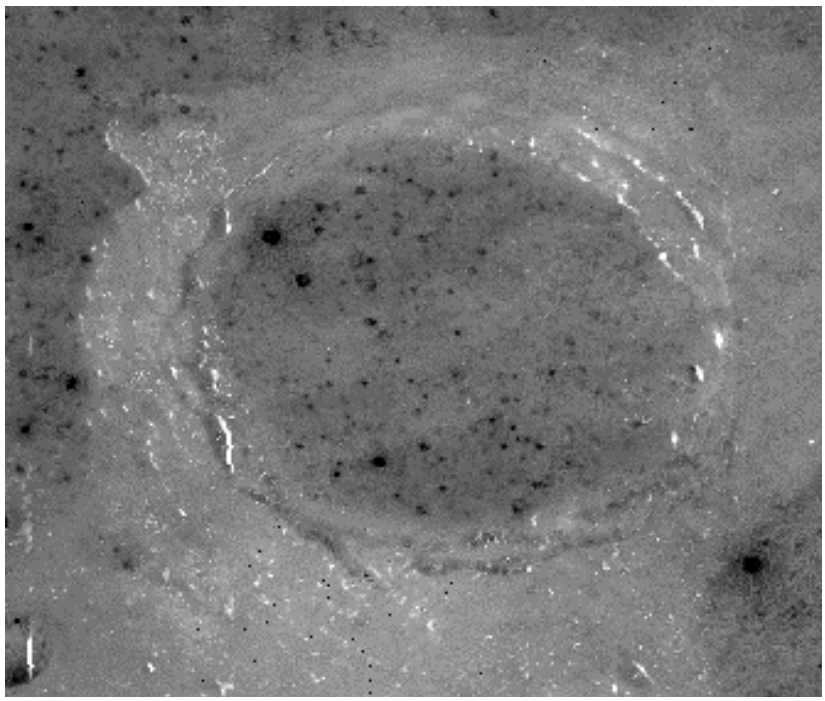

Figure 9e: Oxygen abundance

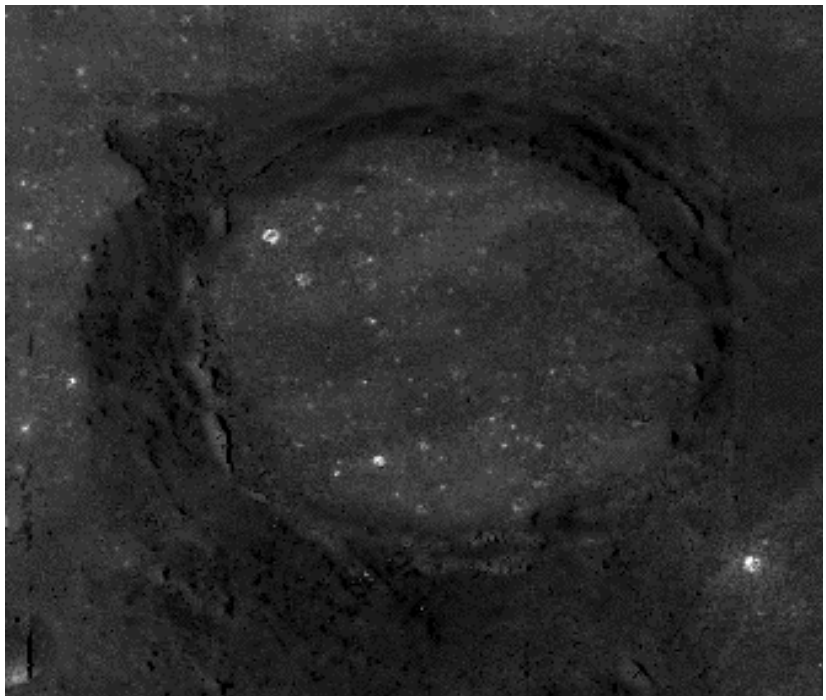

Figure 9f: titanium abundance

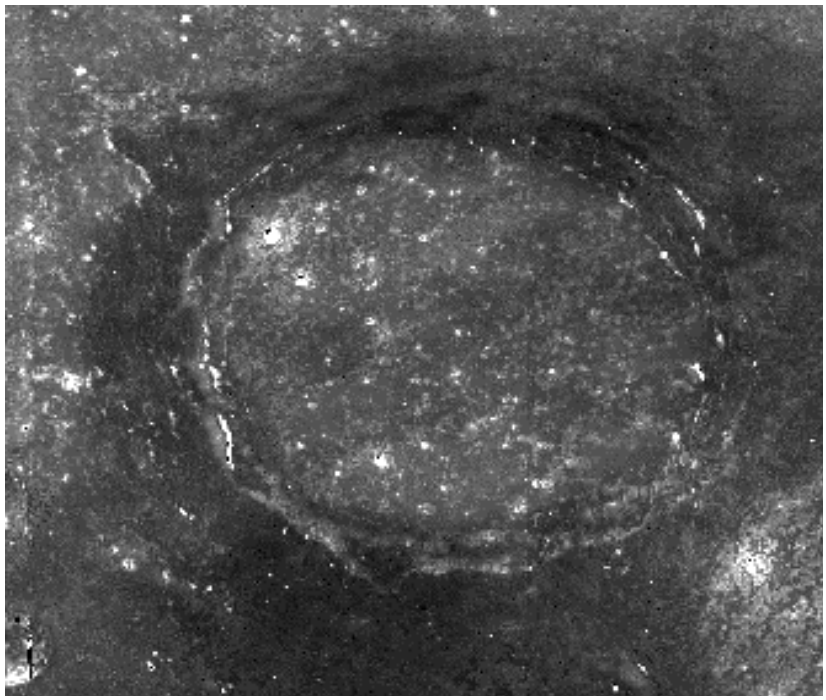

Figure 9g: Magnesium/Aluminum Ratio

The Keck telescopic data are described and are available here:

http://pds-geosciences.wustl.edu/missions/lunarspec/

Crater peak measurements over a spatial area of 5-10 km were chosen as the basis of the calibration because of the geographic certainty that the same geographic area was being compared between Keck and Clementine data after conversion of the Keck data to bidirectional reflectance. A linear regression of the Clementine vs Keck continuum divided spectra for each band was plotted with the slope of the regression line yielding the gain correction and the intercept yielding the offset correction. These coefficients are given in the Appendix of this paper. As the next step in the analysis of the south rim, principal component images were made from the data set of the five UVVIS Clementine images and the first three principal component images were assigned to the red, green and blue channels of Figure 8 below. This composite principal component image appears to show quite a lot of compositional diversity within the larger south rim red spot area. This is shown well in the normalized, continuum divided spectra of this area (Figure 7b).

Discussion

Archimedes crater was studied using spectral maps generated from Clementine UVVIS+NIR image data calibrated using the standard USGS calibration, the Lucey telescopic adjustment of this calibration, and a Keck telescopic calibration based on eight crater peaks. The prominent "red spot" anomaly on the south rim of the crater has long been felt to be produced by pyroclastic debris. Absorption trough parameters measured using the standard USGS, the Lucey, and our Keck eight crater peak calibration all produced very similar results. The FWHM and OMAT spectral maps produced in this study did support this conclusion. The FWHM map shows a wider absorption trough width at the south rim deposit which is consistent with the presence of a significant olivine component within the basalt. The darkness of the south rim deposit on the OMAT image is consistent with pyroclastic material which would appear to be primarily basaltic rather than volcanic glass based on other factors described below. Spectral maps showed that the south rim deposit has a band center of about 940 nm in the USGS and Keck eight peak calibrations, with a band depth of roughly 3 to 5 percent. The Lucey calibration shows this band center to be a bit closer to 900 nm. All calibrations show a second asymmetric, broad and shallow trough with band center above 1000 nm. This finding by itself could be consistent with the presence of an additional component consisting of either pyroclastic glass material, clinopyroxene, olivine or a mixture of these (Hawke, 1989).

The trough data support a Group 1 pryoclastic deposit as described by Lucey et al., 1984. Spectra for Group 1 deposits resemble those of highlands terrain. They suggest felsic composition with a minor mafic component dominated by orthopyroxene (Gaddis , Lunar Pyroclastic Volcanism Project). According to Gaddis, although compositional variation is seen within different Group 1 deposits, most appear to be mixtures of highlands-rich rock and glass-rich juvenile material with small amounts of basaltic caprock material. Figure 9a through 9g show elemental abundance data calculated by the method described in Wöhler et al. 2009 but using the Keck 8 peak calibration of Clementine UVVIS+NIR data. The wt % range for the Figures is as follows: aluminum (0-20 wt %), calcium (2-18 wt %), iron (0-25 wt %), magnesium (0-16 wt %), oxygen (40-47 wt %) and titanium (0-6 wt %). The Mg/Al ratio is lower than would be expected for a volcanic glass in the south rim deposit area. The elemental abundance values for the south rim deposit of Archimedes are reported in Table 1a.

The remainder of the crater rim was largely composed of gabbroic material consistent with medium K Fra Mauro basalt breccia. The most gabbroic area appeared to be the north rim of the crater. The crater interior was flooded with mare basalt easily identified by its band center beyond 1000 nm and this basalt was also present outside the crater in the spectral maps produced. The 2000 nm/1500 nm ratio image favors the presence of an olivine bearing lithology at the south rim anomaly and also near the north rim of Archimedes. The presence of significant amounts of volcanic glass appears to be unlikely based on the low Mg/Al ratio.

It is not clear exactly what causes the ultraviolet absorption in the south rim deposit. There doesn't appear to be any common thread linking lunar red spot features in this regard and the cause may be multifactorial with significant roles played by morphology, rock/mineral composition, and maturation. Theories put foward over the years include the presence of an exotic non-highlands component or the presence of a volcanic glass, but the answer does not seem to be straight foward. Among the various glass types, orange glass can show ultraviolet absorption but typically is associated with a fairly high titanium content. However, a wide variety of different volcanic glasses appear to exist on the moon, each with its own spectral personality. Even so, the Mg/Al ratio calculated above is less than 1.0 and would not be consistent with a volcanic glass. Most volcanic glasses have Mg/Al ratios in the range of 1.7 to 3.3. Also, the mineral composition of the red spot area may be diverse based in part on the composite principal component image shown in Figure-7. One possibility is that the south rim deposit might consist of an MKFM (medium potassium fra mauro basalt) type of basalt having some olivine and orthopyroxene content. Such basalts are KREEP basalts and are entitled to the enriched

thorium content known to be present in this deposit. The elemental abundances for MKFM basalts are intermediate between the low and high K basalt values listed below (see Wilhelms, 1987)

Table 1a: Elemental Abundances

Ca	Al	Fe	Mg	Ti	O
9.7%	12.1%	6.5% (9.4% using Lucey algorithm)*	6.0%	0.8% (0.5% using Lucey algorithm)*	44.6%

(*) Lucey et al. , 2000. Lunar iron and titanium abundance algorithms based on final processing of Clementine ultraviolet-visible images. J. Geophys. Res. 105(E8), 20297-20306.

Table 1b: Small Pyroclastic Deposit Groups (after Coombs and Hawke, 1992)

Pyroclastic Deposit Groups	**Band Center**	**Band Depth %**	**Trough Symmetry**	**Composition**	**Examples**
Group 1	930 nm to 950 nm	4 to 5	asymmetric with a "check mark" shape	mainly highlands type material (feldspar lithology with orthopyroxene as major mafic component) with minor amounts of olivine, clinopyroxene or glass	pyroclastic deposits in or near Atlas, Franklin, and Grimaldi craters
Group 2	960 nm or more	near 7	somewhat symmetric	resembles mature mare basalt with calcium rich clinopyroxene dominant (plug rock)	pyroclastic deposits near Aristoteles crater and on the Aristarchus Plateau
Group 3	1000 nm	5 to 7	asymmetric. trough is broad and is composed of multiple bands	dominant mafic components are olivine and orthopyroxene sometimes with a glass or other minor component	pyroclastic deposits in or near J. Herschel, Alphonsus and Cruger craters

Table 2: Volcanic pyroclastic glasses

Color	Band Center	% Fe Content	% Ti Content	Spectral Slope
orange	1000nm, 1800 nm	high	high	red slope UV shoulder
green	1080nm, 1700 nm	high	low	neutral slope
black	600 nm, 1000 nm, 1800 nm	high	high	blue slope ilmenite trough at 600 nm

Table 3a: Fra Mauro Type Basalts

	SiO_2 wt%	Al_2O_3 wt%	CaO wt%	FeO wt%	MgO wt%	Other wt%
low K	47	23	12	10	11	3.5
high K	53	16	10	10	6	3.5

Table 3b: Fra Mauro Type Basalts

	Si %	Al %	Ca %	Fe %	Mg %
low K	22	14	9	8	7
high K	25	10	7	8	4

References:

Blewett DT and Hawke BR (2001) Remote sensing and geologic studies of the Hadley-Appenine region of the moon. Meteoritics and Planetary Science. 36. pp. 701-730.

Blewett DT; Hawke BR; and Lucey PG (1998) A spectral study of the Hadley-Appenine region of the moon. Lunar and Planetary Science XXIX abstract # 1339.

Charette MP; Taylor SR; Adams JB; and McCord TB (1977) The detection of soils of Fra Mauro basalt and anorthositic gabbro composition in the lunar highlands by remote spectral reflectance techniques. Proc. Lunar Sci. Conf. 8th p. 1049-1061.

Coombs CR and Hawke BR (1992) Pyroclastic deposits on the western limb of the moon. Proceedings of Lunar and Planetary Science. Lunar and Planetary Institute. 22, pp. 303-312.

Evans R; Wohler C; and Lena R (2009) Analysis of absorption trough features using Clementine UVVIS+NIR imagery. Lunar and Planetary Science 40th. abstract #1093.

Evans R; Wohler C; and Lena R (2009) Spectral Mapping Using Clementine UV-Visible-NIR Data Sets: Applications to Lunar Geologic Studies. Selenology Today. 14, pp. 1-70.

Gaddis LR. Lunar Pyroclastic Volcanism Project. (Research Report)

http://astrogeology.usgs.gov/Projects/LunarPyroclasticVolcanism/lunpyroWebresrpt.html

Gaddis LR; Staid MI; Tyburczy JA; Hawke BR; Petro NE (2003) Compositional Analysis of Lunar Pyroclastic Deposits. Icarus 161, pp. 262-280.

Gillis JJ and Jolliff BL (1999) New Views of the Moon II. Lunar and Planetary Institute, 18.

Hawke BR; Lawrence DJ; Gillis JJ; Blewett DT; Lucey PG; Peterson CA; Smith GA; Spudis PD; and Taylor GJ (2003). Spectral Anomalies in the Imbrium Region of the Moon. Lunar and Planetary Science XXXIV abstract # 1545.

Hawke BR (1978) Chemical mixing model studies of selected lunar regions. Lunar and Planetary Institute. 9, p. 474-476. 23

Hawke BR and Lucey P (1984) Spectral studies of the Hadley-Appenine Region (Apollo 15): Preliminary Results. Lunar and Planetary Science Conference, p. 352-353. 1179.pdf

Hawke BR (1989) Remote sensing and geologic studies of lunar dark mantle deposits: a review. Lunar and Planetary Institute Workshop: Volcanic Glasses: Scientific and Resource Potential (held October 10-11, 1989 in Houston, Tx) pp. 34-40.

Le Mouelic S, Langevin Y, Erard S (1999) The distribution of olivine in the crater Aristarchus inferred from Clementine NIR data. Geophysical Research Letters 28(9) pp. 1195-1198.

Lucey PG; Gaddis L; Bell J; and Hawke BR (1984) Near-infrared spectral reflectance studies of localized lunar dark mantle deposits. Planet. Geosci. 15, pp. 495-496.

Lucey PG, Blewett DT, and Jolliff BL (2000) Lunar iron and titanium abundance algorithms based on final processing of Clementine ultraviolet-visible images. J. Geophys. Res. 105(E8) 20297-20306.

Wilhelms, D (1987) Geologic History of the Moon, Chapter 8 p. 140. (available at ser.sese.asu.edu).

Wöhler C, Berezhnoy A, Evans R (2009) Estimation of lunar elemental abundances using Clementine UVVIS+NIR data. European Planetary Science Congress. EPSC abstracts, volume 4.

Acknowledgements:

Figure 1a is used here with the permission of Meteoritics and Planetary Science.

Figure 1b is used here with the permission of Dr. B. Ray Hawke.

Special Acknowledgement: The authors would like to thank Raffaelo Lena (GLR Group) for assistance with calculations and suggestions for improving the manuscript.

Appendix

Gain and Offset coefficients for Lucey and Keck 8 Crater Peak Calibrations

Table 4

Keck 8 crater peak calibration:(must be applied only to continuum divided spectra)

Band	Keck 8 Peak Calib. Gain	Keck 8 Peak Calib. Offset
.75 micron	1	0
.9 micron	0.652077	0.334652
.95 micron	0.73328	0.25725
1.0 micron	0.658683	0.330151
1.1 micron	0.787658	0.206805
1.25 micron	0.6115316	0.385579
1.5 micron	1	0
2.0 micron	0.263676	0.697133

Table 5

Lucey Aristarchus Plateau Gain and Offset Calibration:

Band	Gain	Offset
0.415	1	0
0.75	1	0
0.9	1.012	-0.0004
0.95	1.036	-0.0008
1.0	1.056	-0.002
1.1	0.87	0.246
1.25	0.854	0.316
1.5	0.792	0.0514
2	0.742	0.0680

Note: The Clementine UVVIS+NIR spectral value for each band is multiplied by the gain and the offset is added to the result